Robotic Transducer Control during High Intensity Focused Ultrasound Treatment of Atherosclerosis

Master Thesis Technical Medicine

By

N.C. Morsink

August 2018

Exam committee

Prof.dr.ir. C.H. Slump

Dr. A.J. Teske

Dr. R. Van Es

Drs. P.A. van Katwijk

Prof.dr.ir. B. ten Haken

UNIVERSITY OF TWENTE.

UMC Utrecht

Abstract

Aims To investigate the feasibility of targeting atherosclerotic plaques noninvasively using a high intensity focused ultrasound transducer and a six degrees of freedom robot.

Materials and Methods Custom robot control software was designed and implemented, enabling 3D transducer translations and orientations in the three orthogonal directions (x, y and z), as well as monitoring and visualization of the HIFU ablation positions. Using a digital indicator, caliper and distance laser, the accuracy and repeatability of the robot and software were investigated. The exerted force by the robot's distal end was quantified using a force gauge. In nine animal experiments, the feasibility of robotic transducer control during noninvasive HIFU surgery for atherosclerotic plaque targeting was demonstrated. A retrospective study on patients previously treated with PTA, stenting or surgical revascularization was performed to determine which patients and artery trajectories are most suitable for HIFU surgery. In 25 patients suffering from PAD, the depths of the common femoral artery, superficial femoral artery and popliteal artery were quantified using magnetic resonance angiography (MRA) data. Lesion presence was quantified using the corresponding radiology reports.

Results 2D and 3D visualizations of each HIFU ablation position, and real-time distance feedback for subsequent ablations was implemented. The robot's accuracy and repeatability were found to be smaller than 0.1 mm for most robot translations and rotations. Robot power at its distal end varied from 70.6 – 105.9 Newton. Retrospective analysis of MRA data showed variation in arterial tortuosity and lesion occurrence between patients. ~30% of the dorsal arterial wall left and right can be targeted using the current transducer.

Conclusion The feasibility of robotic transducer positioning with custom robot control software was demonstrated. This research is a first step towards the clinical implementation of the robotic HIFU surgery approach for atherosclerosis, and we hope that it may eventually lead to a standardized noninvasive treatment option for patients suffering from PAD.

Preface

Beste lezer,

Voor u ligt het resultaat van een jaar afstuderen bij de Cardiologie in het Universitair Medisch Centrum Utrecht, ter afronding van de Master Technical Medicine aan de Universiteit Twente. Met veel plezier blik ik terug op het afgelopen jaar. De expertise van collega's en betrokkenen zijn in dit proces onmisbaar geweest en ik wil de mensen die op enige wijze hebben bijgedragen aan de totstandkoming van deze thesis graag bedanken.

Beste René, ongeveer 1,5 jaar geleden ben ik onder jouw begeleiding begonnen met een project omtrent de Microsoft HoloLens. Mijn interesse voor de (experimentele) cardiologie is toen gewekt door het innovatieve karakter van de vele lopende projecten. Deze periode mondde uit in een afstudeerjaar waarbij ik ontzettend veel heb geleerd. Met name kritisch zijn naar mijn eigen werk, onderbouwen van mijn ideeën, laagdrempelig proberen, en altijd vooruit willen, zijn leerontwikkelingen die ik meeneem. Dank voor deze waardevolle ervaring!

Beste Arco, naast de klinische activiteiten heb je tijd gemaakt om het onderzoek inhoudelijk van feedback te voorzien en de uitwerking ervan te beoordelen tijdens de experimenten. Ik acht je klinische input zeer waardevol en ik wil jou hartelijk danken voor je tijd en feedback het afgelopen jaar!

Beste Kees, ik heb de afgelopen twee jaar genoten van de kritische feedback en bijkomende scherpe kanttekeningen, van de bijschriften, referenties en interpunctie, tot inhoudelijke feedback. De koppeling van de technische aspecten aan de klinische uitwerking acht ik zeer waardevol, evenals de boodschap dat ik het vooral leuk moeten voor mezelf! Dit heeft me gemotiveerd met speelse gedrevenheid bezig te blijven.

Beste Paul, vanaf het begin van mijn studieperiode in 2011, en in het bijzonder de afgelopen twee jaar, heb je mij begeleid in mijn persoonlijke en professionele ontwikkeling. Ik ben dankbaar voor je vrije manier van aanpak, doelgerichte vragen, en gedrevenheid om ons te helpen ontwikkelen tot volwaardig professional en persoon. Je werkwijze heeft mijn openheid en reflectie gestimuleerd, en heeft ervoor gezorgd dat ik vooruitstrevend bezig ben gebleven met mijn eigen ontwikkeling.

Ik wil prof. P.A.F.M. Doevendans, prof. G.J. de Borst, dr. C.E.V.B. Hazenberg en dr. F.J.B. Slieker van de cardiologie en vaatchirurgie bedanken voor de klinische input en betrokkenheid. Ik wil de betrokkenen van de International Cardio Corporation en Design Solutions Inc. bedanken voor het meedenken over de positionering, software-verbeteringen en het verschaffen van de benodigde specificaties, en in het bijzonder David Lee, die meerdere experimenten heeft meegedraaid.

Joyce Visser, Martijn van Nieuwburg, en Marlijn Jansen, dank voor jullie begeleiding tijdens de dierexperimenten, de feedback en lekkere broodjes het afgelopen jaar. Evelyn Velema wil ik bedanken voor het beschikbaar stellen van de benodigdheden in het lab. Ik wil Ronald Groenemeijer bedanken, die - veelal met spoed - voor de nodige ICT-faciliteiten heeft gezorgd. Jesse Bosma, Jeroen van den Berg en Ernest Boskovic wil ik bedanken voor het meedenken over de robotexperimenten en het beschikbaar stellen van de benodigde meetapparatuur.

Onmisbaar zijn de collega's uit 'de Villa' geweest. De vele potjes schaak, borrels en dagelijkse clichés hebben bijgedragen tot een ontzettend leuk jaar, met als hoogtepunt het memorabele congres in Barcelona. Ik wil jullie tevens bedanken voor de tussentijdse input en persoonlijke feedback, Marijn in het bijzonder als studiegenoot en directe collega binnen dit project.

Tot slot wil ik mijn ouders en broertje bedanken, die geduldig hebben uitgekeken naar dit moment. Zonder jullie steun en begrip was ik niet zover gekomen. Een goed gesprek en een pilsje met mijn goede vrienden is tevens onmisbaar geweest voor de nodige ontspanning en motivatie, thanks guys!

Dank allen voor jullie bijdrage en veel plezier met lezen,

Chiron

Table of contents

Chapter 1 Introduction

1.1 Atherosclerosis and Atherothrombosis

Cardiovascular disease (CVD) causes more than 4 million deaths each year across Europe, accounting for 45% of all deaths[1]. Coronary heart disease and cerebrovascular disease were the most common cause of CVD deaths in 2016, accounting for 1,8 million and 1,0 million deaths, respectively[1]. The majority of fatal accidents are due to vascular obstructions, leading to acute coronary syndromes (unstable angina, acute myocardial infarction, and sudden cardiac death), peripheral arterial disease (PAD), ischemic stroke, and transient ischemic attacks[1,2].

Vascular obstructions can be caused by the formation of atherosclerotic plaques and thrombi. Systemic atherosclerosis often is the underlying cause that affects large and medium sized arteries[2]. PAD is defined as atherosclerosis of the aorta, iliac and lower extremity arteries, and is associated with substantial morbidity and mortality[3–5]. Subendothelial accumulations of cholesterol macrophages, calcium and fibrous tissue lead to fatty streaks which thicken the subintimal region, i.e. atheroma. Slowly growing stable or unstable atherosclerotic plaques lead to any degree of stenosis due to a decreased lumen by either atheroma or thrombus formation (**Figure 1.1**). Unstable plaques can trigger thrombus formation by rupture or erosion of the plaque, leading to endothelium laceration and the aggregation of platelets, fibrin, clotting factors, and cellular elements of blood that attach to the inner layer of the arteries wall. This is an emergency clinical phenomenon eventually leading to a chronic total occlusion, which always develops from an atherosclerotic plaque, or to acute ischemia in the distal vascular territory caused by an embolus[6]. Progressive atherosclerotic plaque growth can be limited or slowed down by blocking the neovasculature and development of the lipid-rich core, thereby limiting subintimal thickening of the arteries wall and subsequent thrombus formation[7].

Primary assessment of patients suffering from PAD is performed by means of patient history and physical examination. Subsequently, computed tomography angiography (CTA) and magnetic resonance angiography (MRA) are used to document the severity, location and hemodynamic importance of the vascular lesions, and to make a plan in case intervention is needed[8].

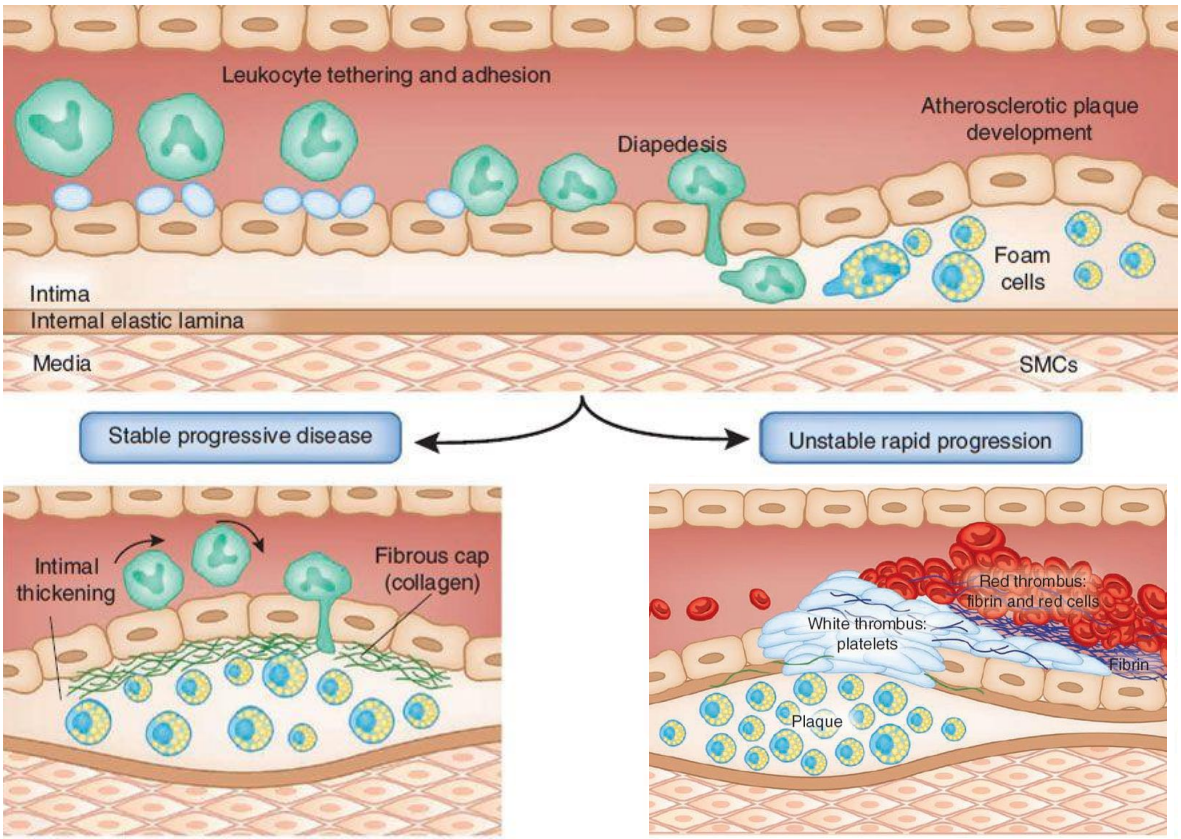

Figure 1.1 Stable and unstable progression of atherosclerotic lesions and the development of arterial thrombosis. The development of atherosclerotic lesions is propagated by leukocyte-platelet and leukocyte-endothelial interactions. During the development of stable progressive atherosclerotic plaques, slow progressive accumulation of proatherogenic leukocytes and foam cells is initiated at sites of atherosclerosis. A collagen-rich fibrous cap stabilizes the plaque. In contrast, the development of a necrotic lipid core, inflammatory infiltrates and a thinning of the fibrous cap are characteristics of an unstable atherosclerotic plaque. Erosion or disruption of the fibrous cap exposes the thrombogenic matrix proteins, thereby promoting the accumulation of platelets and the generation of local fibrin. The atherosclerotic lesion progresses as the thrombus is incorporated into the plaque during re-endothelialization of the lesion. Due to the low flow recirculation on the downstream margin of the developing thrombus, red blood cells and fibrin accumulation occurs and forms a 'red thrombus', further occluding the vessel lumen and eventually leading to a chronic total occlusion. Image and caption adapted from Jackson[9].

The degree of luminal stenosis and patient's symptomatology primarily determine the best treatment option for each patient[10]. Smoking, hypertension, hypercholesterolemia, and type 2 diabetes account for the majority of risk associated with the development of clinically significant PAD[11]. Noninvasive interventions that can beneficially influence atherosclerotic progression include lifestyle modifications, such as dietary control, exercise, and smoking cessation, as well as pharmacotherapy, including lipid-lowering, antihypertensive, antiglycemic, and antiplatelet drugs. However, pharmacotherapy may cause adverse side effects due to its systemic manifestation[2]. Moreover, a significant percentage of patients fail conservative therapy due to poor compliance and varying impact on functional capacity, as shown in patients suffering from claudicatio intermittens[12]. Finally, aforementioned noninvasive interventions only slow the progression of atherosclerosis and some degree of progression is typically observed.

Invasive treatment options include revascularization of the arteries by either surgical endarterectomy or surgical bypass. The associated morbidity and mortality, the relatively high costs and high procedural times form the major drawbacks of invasive open surgery, and preclude its routine use[13,14]. Endovascular approaches, e.g. percutaneous transluminal angioplasty and/or selective stenting, are limited due to the potential detachment of fragments, dissection, vessel damage, elastic recoil, restenosis, and infection, despite their high rate of success[13]. Moreover, entrance to the true lumen may not even be achieved, especially in the treatment of CTOs[14]. Millimetric removal devices allow for endovascular cleansing of the artery lumen. However, their therapeutic success is still limited and significant improvements are needed for full clinical implementation of these wired technologies, which are difficult to operate in the complex human vasculature[13]. The limitations bound to aforementioned high-end therapeutic strategies stress the need for considerable improvement in the treatment of vascular obstructions, preferably non invasively[13].

High-intensity focused ultrasound (HIFU) is a noninvasive thermal treatment strategy capable of producing necrosis within plaque tissues in peripheral vessels while preserving the overlying endothelium, potentially offering a solution in the search for noninvasive and nonionizing treatment options for PAD[15].

1.2 High intensity focused ultrasound

HIFU enables noninvasive treatment through localized thermal lesion formation that has become a promising and in some applications a well-established alternative to surgical resection and other treatment forms over the past 20 years[16]. Its clinical application in the treatment of atherosclerosis is currently under investigation.

1.2.1 HIFU therapy for the treatment of atherosclerosis

Focused ultrasound (US) with relatively high intensities (~1000 W cm^{-2}) can lead to coagulative necrosis[15,17] without significant biological damage to intervening and surrounding tissue, with proper choice of operating frequency and transducer design[18,19]. The temperature increase in the focal area is proportional to the absorptive properties of the target tissue, which increases with frequency and the time-averaged HIFU intensity. HIFU exposures of 55 °C or higher maintained for 1 s or longer will generally lead to immediate cell death by coagulative necrosis in most tissues[20–22]. Despite rapidly increasing tissue temperatures in the focal area, surrounding and intermittent tissues are not affected as HIFU energy can be focused into small, confined volumes with temperatures outside its focus kept at levels that are not cytotoxic[23]. Moreover, normal vascular wall tissues remain intact as they are rich in elastic fibers, thereby allowing them to buffer the thermal effect of US[24–27]. At last, the convective removal of heat by the blood flow and the perfusion of the large vessels in vicinity of the target area also buffer the thermal HIFU effect at the level of the endothelium[28].

As shown in early animal and *in vitro* studies, US can selectively destroy tissues lacking normal collagen and an elastic fibrous skeleton, such as thrombi and atherosclerotic plaques[24–27]. The growth dynamics of atherosclerotic plaques, entailing neovascularization and build-up of lipid-rich core, suggest that a plaque may respond to localized thermal therapy[29]. Atherosclerotic plaque growth is blocked by occluding the neo-vessels, while preserving the overlying endothelium. Classical thermal HIFU lesions are ellipsoidal, paralleling the direction of the US propagation, measuring about 1.5 – 2 cm in length and about 1.5 – 2 mm in width when produced by a typical clinical 1.5 MHz HIFU field (**Figure 1.2**)[30]. Two hours after HIFU exposure, such lesions typically consist of a core which is completely coagulated, and a surrounding rim-like area with glycogen-poor cells that usually die within 48 hours[31,32]. Progressive plaque growth is limited or slowed down and the ablated plaque may shrink through the formation of granulation tissue, infiltration of fibroblasts and finally retraction and scar formation[31,33].

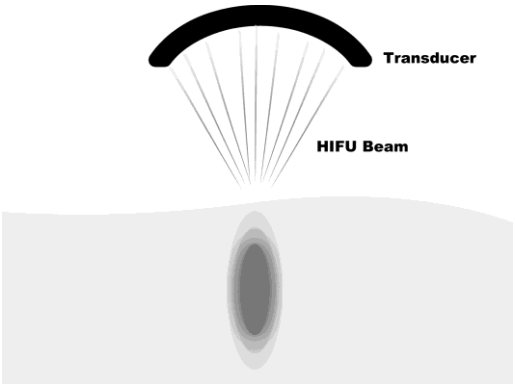

Figure 1.2 Thermal effect of HIFU: Ellipsoidal lesion formation at the focal point paralleling the US wave pathway. The incident focal US waves are absorbed and converted into heat at the HIFU focus, resulting in thermal ablation of the target tissue. Image reproduced from Shehata et al.[15]

Compared to other thermal ablation techniques, such as cryotherapy, laser ablation, microwave coagulation, and RF ablation, the major advantages of HIFU therapy are its noninvasive and nonionizing characteristics, as well as the absence of long-term cumulative effects, and fast, confined lesion formation[34]. HIFU allows for accurate, tailorable treatment margins to ablate tissues within the body[16,35]. HIFU therapy is therefore much less traumatic for the patient compared to other treatment strategies, and may shorten hospitalization times and decrease treatment costs[16].

Pitfalls of HIFU therapy may include long procedural duration in case of large targeted volumes, local pain after treatment in some cases, and the need of general anesthesia, which can be hazardous in patients with serious conditions[34]. In one study, patients treated for local body tumors only received HIFU therapy six months after a myocardial infarction to ensure good cardiac reserve that can tolerate anesthesia[15]. It was advised that hypertension and diabetes should be under control, and blood glucose levels should be between 5.6 and 11.2 mmol/L before treatment. Additionally, treatment should be performed early in the morning, and all patients should be fasting overnight to help for safe anesthesia[15].

Complications of HIFU therapy include local edema, skin toxicity, and interfering objects affecting the ability to treat[36]. HIFU cannot be applied to tissues that are not compliant with US, such as lung and bone[34]. Initial therapeutic limitations consisted of the difficulty of monitoring changes in temperature and tissue mechanical properties[36,37]. It was not possible to control precise thermal exposure upon lesion formation. Currently, dual-mode ultrasound arrays (DMUAs) allow for image-guided HIFU surgery with robust image-based identification of target tissue to monitor HIFU lesion formation[38].

1.2.2 HIFU therapy using dual-mode ultrasound arrays

Utilizing DMUAs in US-guided HIFU therapy allows for imaging and treatment using the same elements. Monitoring of temperature changes in tissues was realized by applying sparse imaging and speckle tracking techniques to the radiofrequency (RF) data that is acquired before, during and after HIFU therapy. Pulse-echo imaging techniques and post-beamforming filtering of the RF data was implemented to visualize HIFU-induced lesions and track lesion formation in real-time. Accurate spatial registration allows for refocusing of the HIFU beams in the presence of large scattering obstacles, such as bone tissue, that may partially obstruct the focus and thus distort the HIFU beam. Finally, DMUAs allow for inherent registration between the imaging and therapeutic coordinate systems[38]. *In vitro* experiments showed accurate temperature and lesion formation monitoring, as well as refocusing around critical obstacles that partially obstruct the HIFU beam[39].

The use of DMUAs for imaging-guided treatment of atheromatous plaques was investigated *in vivo*[38]. Diagnostic US was used to verify the presence of plaque in the femoral artery of familial hypercholesterolemic swine, while the therapeutic transducer was used for the delivery of discrete HIFU shots with an estimated focal intensity of 4000 to 5600 W/cm^2 and 500 to 2000 ms duration, for several transverse plaque slices in direction of the target artery. Results showed confined plaque tissue damage, without damage to the endothelium. Aforementioned study provided the first demonstration of real-time DMUA and diagnostic imaging-guidance in targeting fine tissue structures for precise lesion formation in the presence of arterial pulsation and tissue motion. A later study proved the feasibility and acute safety of using noninvasive HIFU with DMUAs to form localized thermal lesions within atherosclerotic plaques, also without damaging the endothelium[40]. This study concluded that further long-term studies are needed to assess how induction of these lesions can modify the progression of atherosclerotic plaques.

Recently, real-time monitoring and lesion formation control utilizing a DMUA system was advanced by real-time signal processing of echogenicity changes during lesion formation, allowing for the cessation or reduction of the HIFU exposure, e.g. intensity and/or time, to prevent overexposure[41]. Uncontrolled volumetric HIFU lesions resulted in significant pre-focal buildup due to excessive exposure from multiple full-exposure HIFU shots, whereas adaptive lesion formation resulted in tissue damage consistent with the size of the focal HIFU spot. Controlled lesions were produced with no evidence of overexposure by stopping or reducing the HIFU exposure in real-time. More-over, underexposure at the target location was also detected using the same DMUA-echo data. This adaptive closed-loop control of lesion formation resulted in lower treatment times while confining tissue damage to the target volume[41].

1.3 Atherosclerotic plaque targeting

To evolve HIFU to a standard treatment modality for atherosclerosis, localization and targeting of atherosclerotic plaques is required. To ensure contiguous lesion formation within plaques, subsequent discrete HIFU shots need to be delivered to multiple transverse planes in direction of the target vessel. Partially overlapping lesions can be formed with adjacent HIFU lesions and through thermal conduction within the substance of the plaque, leading to a confluent ablated zone[40]. In the treatment of atherosclerotic plaques, transverse treatment planes are typically spaced 1 mm apart to ensure partially overlapping HIFU lesions across treatment planes (**Figure 1.3**). A HIFU shot is defined as HIFU energy delivery in one focal spot. Depending on the diameter of the artery and plaque size, 6 to 8 HIFU shots need to be delivered in the target area and 25 to 40 planes are typically treated.

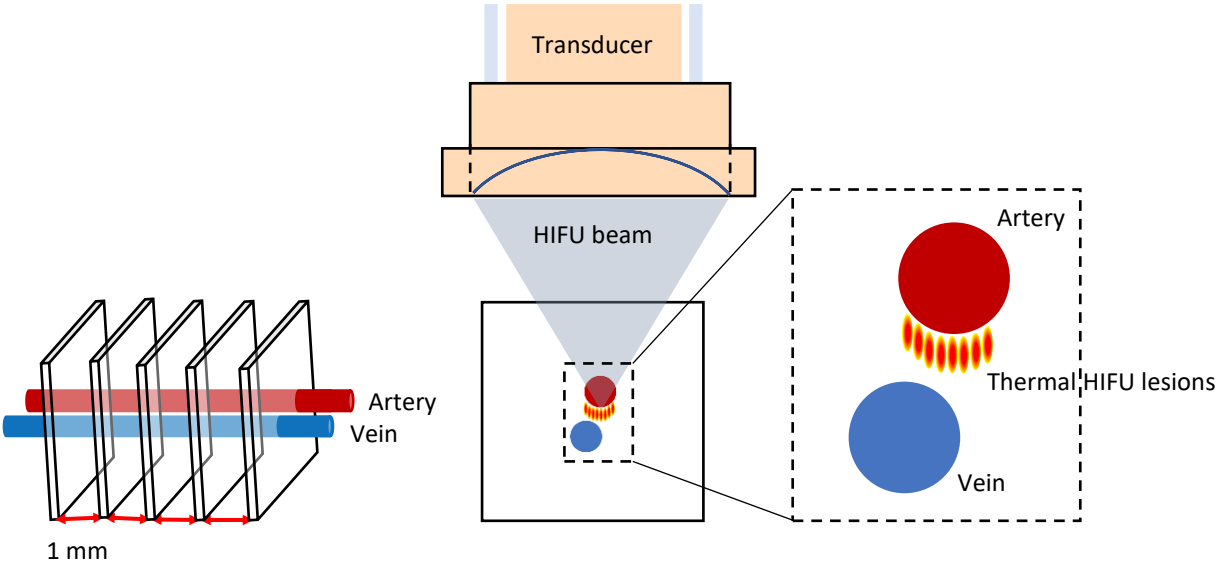

Figure 1.3 Targeting the arterial wall with high intensity focused ultrasound. **Left**. Transverse treatment planes (side view) in direction of the target artery spaced 1 mm apart. **Right.** 2D transverse treatment plane with thermal HIFU lesions. HIFU = high intensity focused ultrasound.

1.3.1 Robotic transducer control

In 1998, a robotic approach to HIFU based neurosurgery was investigated, aiming to simultaneously move and focus the HIFU probe, thereby minimizing off-focal hot-spots and cavitation[42]. Over the last decade, a hybrid control approach in HIFU therapy has been studied in the form of a noninvasive medical robot called Focused Ultrasound Surgical Robot, either for Breast Surgery (FUSBOT-BS) or Urological Surgery (FUSBOT-US)[43,44]. The accomplished compensated end-point accuracy of the robotic system was within 0.5 mm. A recent study developed an experimental US imaging-guided robotic HIFU ablation system for tumor treatment, aiming to integrate the technologies of US imaging-guidance, robotic positioning control, and HIFU treatment planning so that the robotic arm can position the DMUA-transducer to ablate the targeted tumors (**Figure 1.4**)[45]. An average positioning error of 1.01± 0.34 mm, and a HIFU ablation accuracy of 1.32± 0.58 mm was found. These studies stress the advantage of robotic HIFU control in positioning and monitoring during HIFU therapy.

1.3.2 Multi-modality imaging

In recent years, multi-modality imaging techniques have been investigated to advance imaging for clinical diagnosis, most commonly including combinations of CT, single photon emission computed tomography (SPECT), positron emission tomography (PET), and MRI. With hybrid imaging approaches, the reliance on image co-registration is reduced as the patient remains in the same position while both data sets are acquired. MR-guided focused US proved to be of significant importance in terms of real-time thermal exposure monitoring and providing excellent soft-tissue contrast for targeting purposes during HIFU procedures[46,47]. Along with the development of advanced FUS transducers, efficacy of MR-guidance can be improved in consideration of new clinical applications, such as moving-organ ablations[48]. A real-time navigation system with US-CT/MRI fusion imaging has shown to be precise for targeting and successful ablation of target tumors, which were undetectable solely using US[49]. It may be useful to combine CT/MRI with the DMUAs integrated imaging mode and thereby advance pretreatment planning, imaging-guidance, monitoring and targeting of atherosclerotic plaques during HIFU treatment[50]. The use of MRA images for pretreatment planning, patient selection and pre- and postoperative assessment of the target area is expected to be of additional value in targeting atherosclerotic plaques.

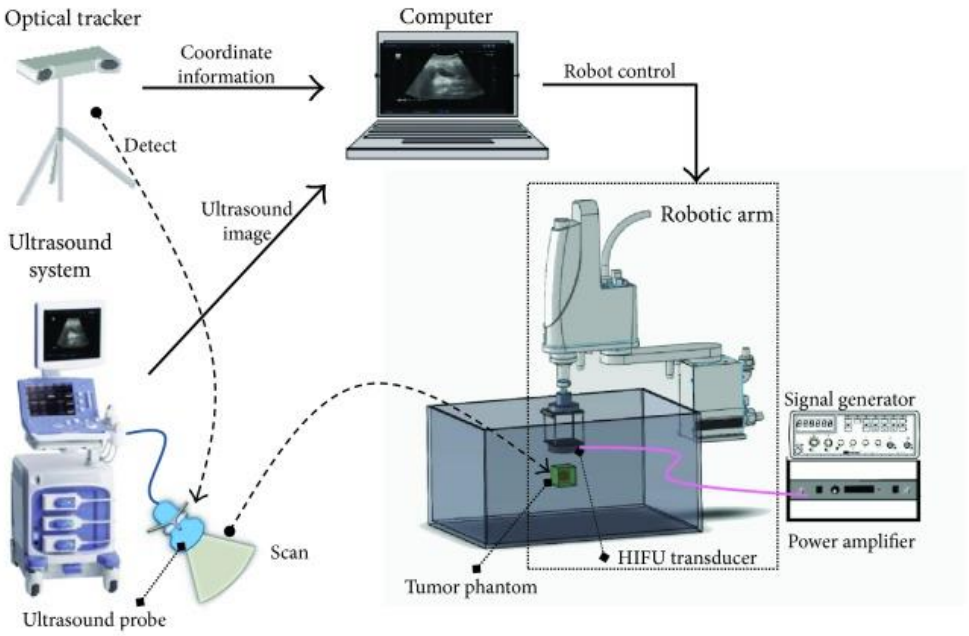

Figure 1.4 "The ultrasound imaging-guided robotic HIFU system", reproduced from An et al.[45]

1.4 Aims

The aim of this project was to optimize localization and targeting accuracy during HIFU treatment of atherosclerotic lesions in the femoral artery using a six degrees of freedom robot. Additionally, the use of pre- and periprocedural MRA imaging will be investigated, as well as the feasibility of treating patients suffering from PAD with HIFU therapy in the future.

Aims

1. To implement robotic transducer control.
    a. Analyze the experimental setup incorporating a DMUA transducer and robot.
    b. Analyze the default and desired robot control.
    c. Investigate the required accuracy and repeatability of robotic transducer control for atherosclerotic plaque targeting.
    d. Investigate the safety and feasibility of robotic transducer control for atherosclerotic plaque targeting.

2. To validate robotic transducer control.
    a. Investigate the safety of robotic transducer control.
    b. Investigate the robot's accuracy and repeatability to ensure contiguous lesion formation during HIFU therapy.
    c. Investigate the feasibility of robotic transducer control *in vivo*.

3. To investigate HIFU targeting of the common femoral artery, superficial femoral artery, and popliteal artery in patients suffering from PAD.

4. To investigate the added value of combining DMUA-imaging with MRA images for targeting and localization purposes.

Chapter 2 Experimental setup and robotic transducer control

2.1 Introduction

During HIFU therapy, subsequent discrete HIFU shots need to be delivered to multiple transverse planes in direction of the target vessel. It is therefore important to precisely position and move the transducer during a HIFU procedure. To advance transducer positioning and improve efficiency during HIFU therapy, a DMUA-transducer is mounted to a six degrees of freedom (DOF) robot. It is hypothesized that using a robot to control the transducer improves the accuracy, monitoring and guidance of atherosclerotic plaque targeting, and thereby increases therapeutic success. It has already been shown that experimental robotic HIFU setups are capable of reliable transducer positioning during therapy, with average system accuracies ranging from 0.1 to 1.01 mm[43–45,51–53]. One study ensures successful targeting of 1 mm volumes with a positioning error of 0.59 ±0.25 mm, and a maximum orientation error of ±2.3°, assuming predictable sound wave propagation[52]. However, aforementioned studies investigated the use of custom-built robotic transducer manipulators with fewer DOFs for other clinical applications, as opposed to utilizing an industrial six-DOF robot to advance atherosclerotic plaque targeting. It is important to define requirements for the successful implementation of the unique robotic HIFU setup and custom transducer control, and subsequently investigate the required accuracy and safety measures.

Aims

The aim is to investigate the requirements of robotic transducer control for successful implementation of localization and targeting of atherosclerotic plaques during a HIFU procedure, using a HIFU system, a DMUA-transducer and a six-DOF robot.

1. Analyze the experimental setup

2. Analyze UR3 robot control
   a. Analyze default robot control using Polyscope
   b. Design and implement custom robot control software.

3. Investigate the required accuracy and repeatability of the robotic transducer control.

4. Investigate the safety requirements with respect to the robotic transducer control.

2.2 Experimental setup

2.2.1 The HIFU system and DMUA transducer

Transducer specifications

The DMUA-transducer (Imasonic Inc., Voray sur l'Ognon, France) is a concave 3.5 MHz, 32x2 phased array with a 50 mm radius of curvature and a fractional bandwidth of ~40%. The element pitch and height are 1.6 and 34 mm respectively, divided in two rows of equal height with inter-row spacing of 0.2 mm. The transducer is capable of operating in a variety of imaging and therapy modes on transmit, and receive on all array elements.

HIFU software

The HIFU software consists of an Image Targeting Control Panel, and a separate Closed-Loop Imaging and Treatment control panel, wherein patient information, the system status and the HIFU research settings are displayed and can be adjusted (**Figure 2.1**). The Targeting Control Panel is used to image with real-time single-transmit focus (STF) or synthetic aperture (SA) imaging. STF imaging is primarily used during therapy to provide high frame rate imaging to monitor the dynamics of lesion formation at the treatment site, whereas SA imaging allows for tracking of the vessel dynamics with higher image quality[54]. STF and SA-imaging settings such as the amplitude, sample width, dynamic range and frame count, can be adjusted in the research settings panel. Prior to HIFU delivery, the transducer cable and thermocouples need to be attached to the HIFU system, which allows for checking the receiving and transmitting HIFU elements and the transducer temperature. Subsequently, SA imaging is required, and the skin region, the therapeutic region of interest and the HIFU focus need to be manually selected (**Figure 2.1**). HIFU delivery settings such as HIFU shot duration, pulse width and amplitude can be adjusted. Subsequently, HIFU prescription shots can be delivered with the configured HIFU amplitude, or sub-therapeutic HIFU shots can be delivered, with 20% of the configured HIFU amplitude and with the closed-loop control (CLC) disabled. After HIFU delivery, the lesion control profile can be opened to assess the HIFU lesion formation and CLC interference.

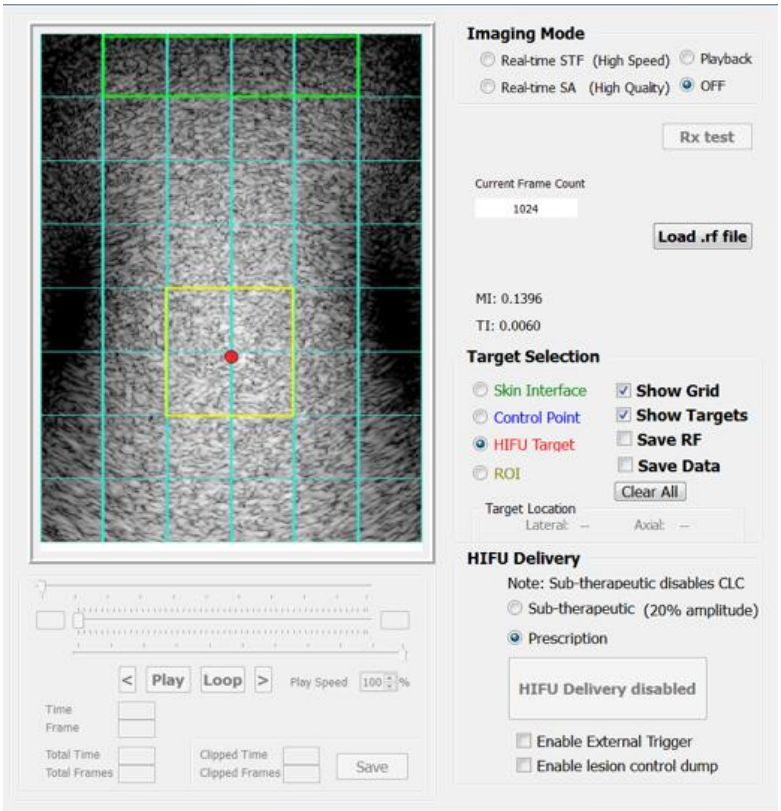

Figure 2.1 Image Targeting Control Panel HIFU software with skin interface, region of interest and HIFU focus selected.

HIFU range, therapeutic operating field and intensity distribution

The optimal HIFU focus is located at 0 mm laterally and 50.1 mm axially, based on the transducer's average radius of curvature, 50.1 mm ±0.05 mm (Measurement report Imasonic Inc., France). The lateral (horizontal) and axial (depth) ranges of the transducer are -15 to 15 mm, and 25 to 65 mm, respectively. The HIFU range is hardware-limited and cannot be changed using the software. The transducer's therapeutic operating field (ThxOF) is an elliptical region around its geometric focus, with an extent of ±7 mm laterally and ±5 mm axially, wherein HIFU therapy is most effective. As HIFU intensity decreases rapidly outside its geometric focus, targeting outside the ThxOF results in unacceptable reduction in focusing gain at the target and may lead to less unequivocal lesions[54]. Targeting outside the ThxOF should therefore not be performed (**Figure 2.2**).

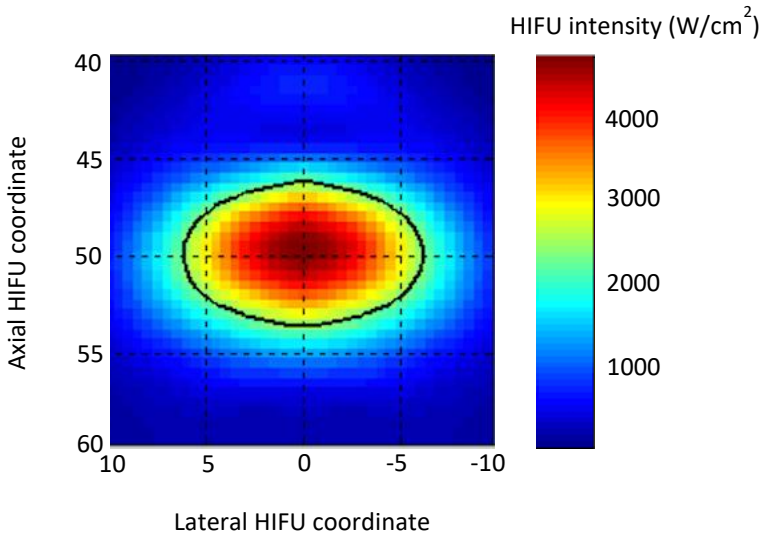

Figure 2.2 HIFU intensity distribution around the transducer's geometric focus (lateral value 0 mm, axial value 50.1 mm).

Bolus cover

To ensure proper contact with the skin surface, a bolus cover is screwed onto the concave-shaped transducer. Degassed water is circulated through the space between the transducer and the membrane of the bolus cover, which needs to be in contact with the skin to ensure US coupling to the region of interest. The distance between the distal end of the concave-shaped transducer and the patient's skin ranges from 15 to 25 mm, depending on how far the bolus cover is screwed onto the transducer (**Figure 2.3**).

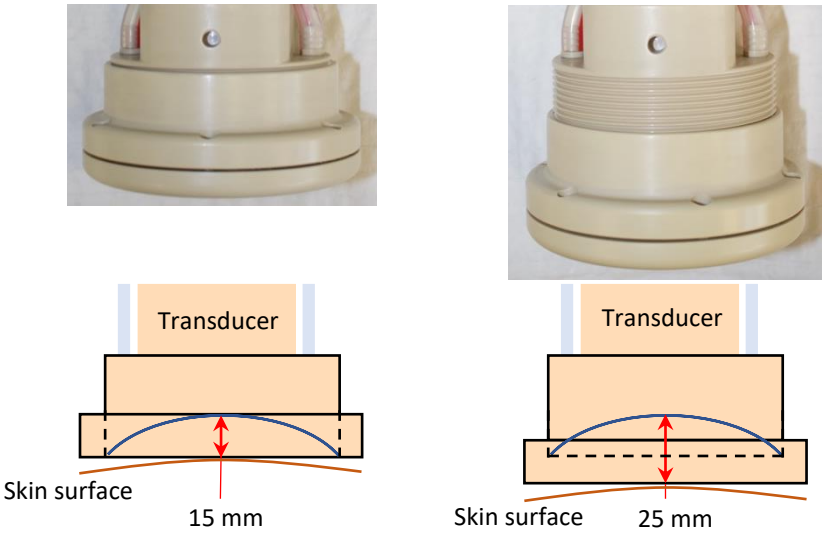

Figure 2.3 Distance between the distal end of the DMUA-transducer and bolus cover. **Left.** Distance with bolus cover screwed on maximally. **Right.** Distance with bolus cover screwed on minimally.

2.2.2 The UR3 robot

The transducer is fixed to a UR3 robot, an industrial robot with 6 rotating joints, weighing 11 kg, and capable of handling a maximum payload of 3 kg in 360-degree rotation on all wrist joints, and infinite rotation on the end joint (**Figure 2.4**)[55]. In robotics, repeatability is defined as the capability to repeatedly return to the same pose under equal circumstances. Repeatability of the UR3 is ±0.1 mm, and its reach radius is 500 mm. Maximum speed of the joints are ±180°/s for the first three joints, i.e. the Base, Shoulder and Elbow, and ±360°/s for the last three joints, i.e. Wrist 1 to 3. The robot's distal end is called the tool, which can move with a maximum speed of 1 m/s.

The UR3s control box facilitates the robot's power supply and has several analog and digital in- and output connections to add custom safety features and control the UR3 with external devices.

The UR3 can be configured, controlled and programmed utilizing Polyscope, the graphical user interface (GUI) installed on the Teach Pendant, a separate 30.48 cm touchpad (**Figure 2.4** and **Chapter 2.3.1**).

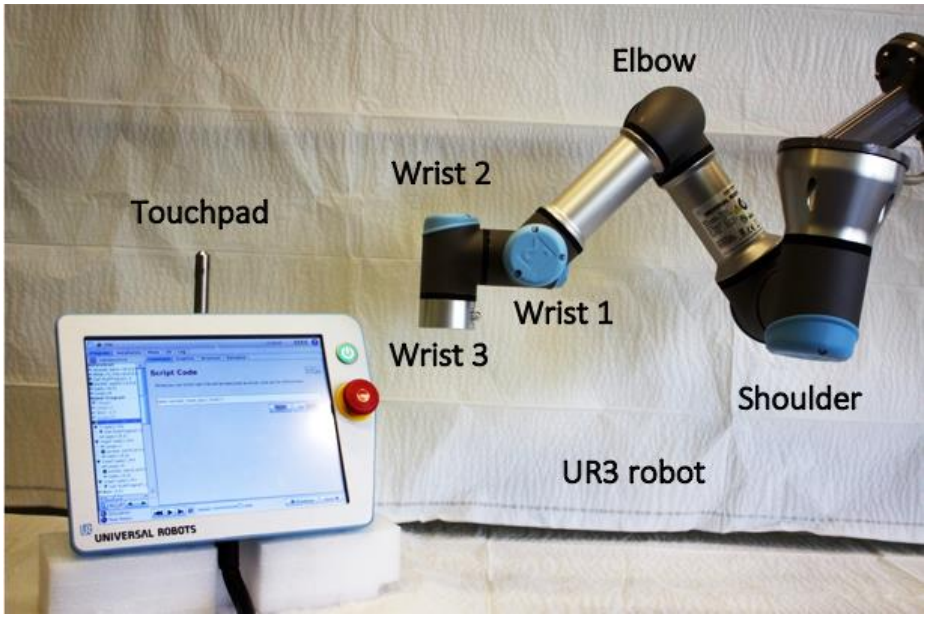

Figure 2.4 UR3 robot with Touchpad.

Custom robot control

To allow for custom robot control of the transducer, and thereby improve positioning and targeting during HIFU therapy, a desktop computer running MATLAB (MathWorks, Natick, MA, USA) is linked to the UR3 robot's control interface through an Ethernet socket connection (**Chapter 2.3.2**). A 3Dconnexion SpaceMouse® Pro (3Dconnexion, Munich, Germany) was linked to MATLAB software to allow for direct 3D navigation of the UR3 robot, using its six-DOF sensor.

2.2.3 Transducer bracket

A manually manufactured bracket is used to mount the DMUA transducer to the UR3 (**Figure 2.5.A**). Its length, width and height are 69.9, 76.2 and 127.0 mm, respectively. Four 6 mm bolts are used to mount the bracket to the distal end of the UR3 robot. The transducer is mounted to the inferior end of the bracket with two 6 mm bolts, where a rectangular gap in the center provides space for the two water tubes and the transducer's controlling cable, which is attached to the HIFU system.

2.2.4 Robot frame

The UR3 robot is fixed to a custom manufactured steel frame, capable of handling the weight of the robot and its payload (**Figure 2.5.B**). The steel frame can be moved and is angle-adjustable, so the configuration of the robot can be changed at its Base. Breaks at the level of the wheels are present to prevent movement of the steel frame and thereby ensure stable positioning.

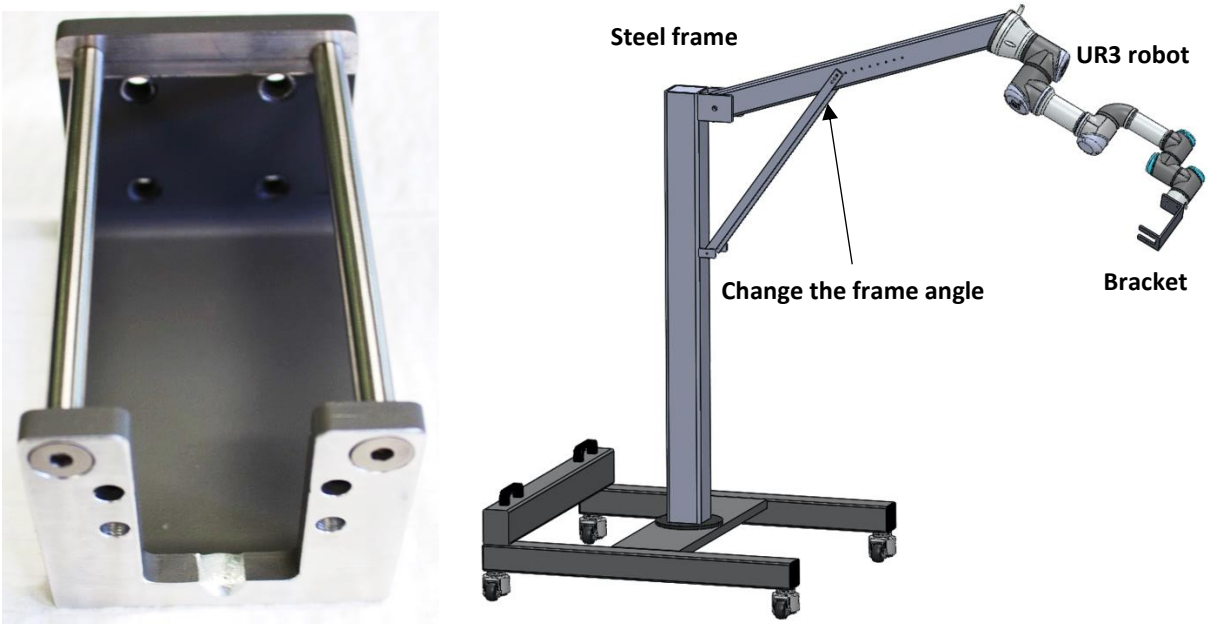

Figure 2.5 A. Inferior view of the bracket. **B.** Angle-adjustable steel frame with UR3 robot and bracket attached.

2.2.5 Water degassing system

A portable water degassing system (FUS-DS-50 Water Degassing System, FUS Instruments Inc., Toronto, Ontario, Canada) is used to produce and circulate degassed water through the water bolus (**Figure 2.6**).

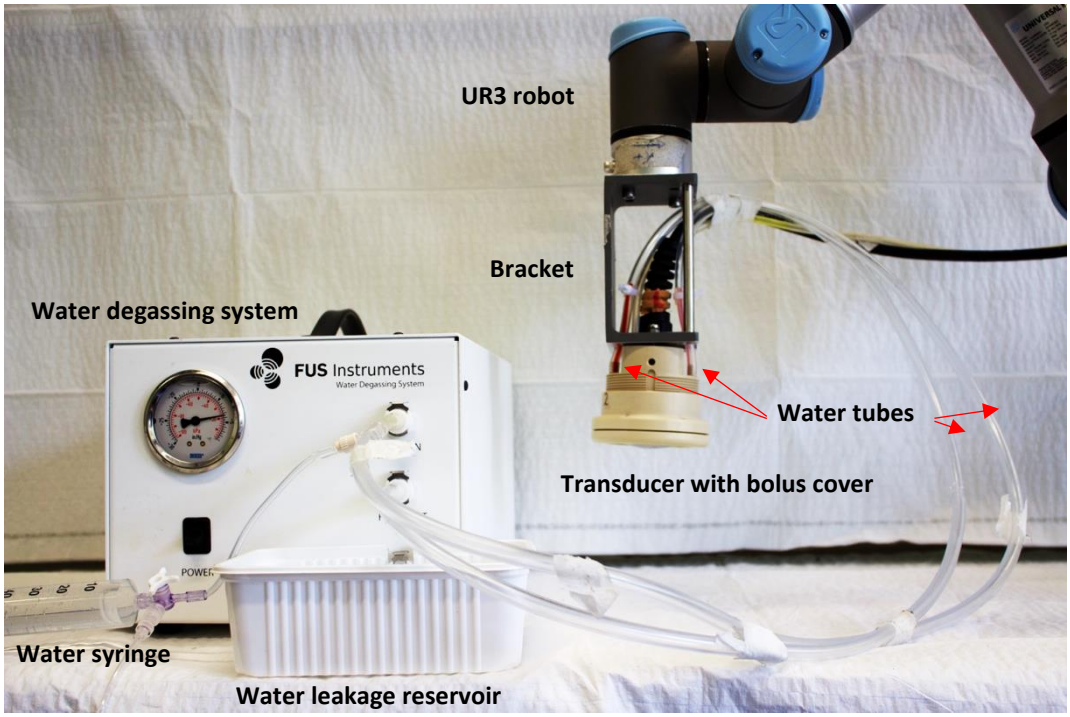

Figure 2.6 UR3 robot with bracket and transducer attached. Two tubes facilitate the circulation of degassed water between the water degassing system and the bolus cover.

2.3 Robot control

The center point at the level of the UR3 robot's end effector is called the Tool Center Point (TCP), and its 3D position is defined as the robot pose, a six-element vector containing x, y, and z-values for both the translation and orientation (

Equation 2.1). The robot can be moved and translated by changing the robot pose, either by using Polyscope or by using external control software.

$$[-166.98 \ -375.92 \ 308.94 \ -0.1596 \ -0.0699 \ -0.1788]$$
$$x \quad y \quad z \quad x \quad y \quad z$$

Equation 2.1 Example robot pose with x, y and z-values for both the translation (blue, mm) and orientation (green, radians), with respect to the robot's base.

2.3.1 Robot control using Polyscope

Using Polyscope, the UR3 can be programmed to move the TCP to specific waypoints, each joint can be controlled separately and a real-time 3D visualization of the UR3 is displayed (**Figure 2.7**). To control the robot during HIFU therapy, Polyscope was preprogrammed to move the UR3 between -10 and 10 mm for the x, y and z-direction in orientation of the tool (**Figure 2.8**). During preclinical testing, this program was experienced to be laborious, as robot motion needed to be configured for all three directions successively prior to the execution of robot motion. Moreover, the range of robot motion was very limited and the robot poses could not be saved. Accessing the 3D real-time UR3 robot visualization from the program was experienced to severely interrupt the workflow, and additional features, such as displaying the linear 3D distance between robot poses, cannot be implemented in Polyscope. Therefore, the requirements of controlling the UR3 robot for atherosclerotic plaque targeting were identified, and custom robot control software was designed and implemented (**Chapter 2.3.2**).

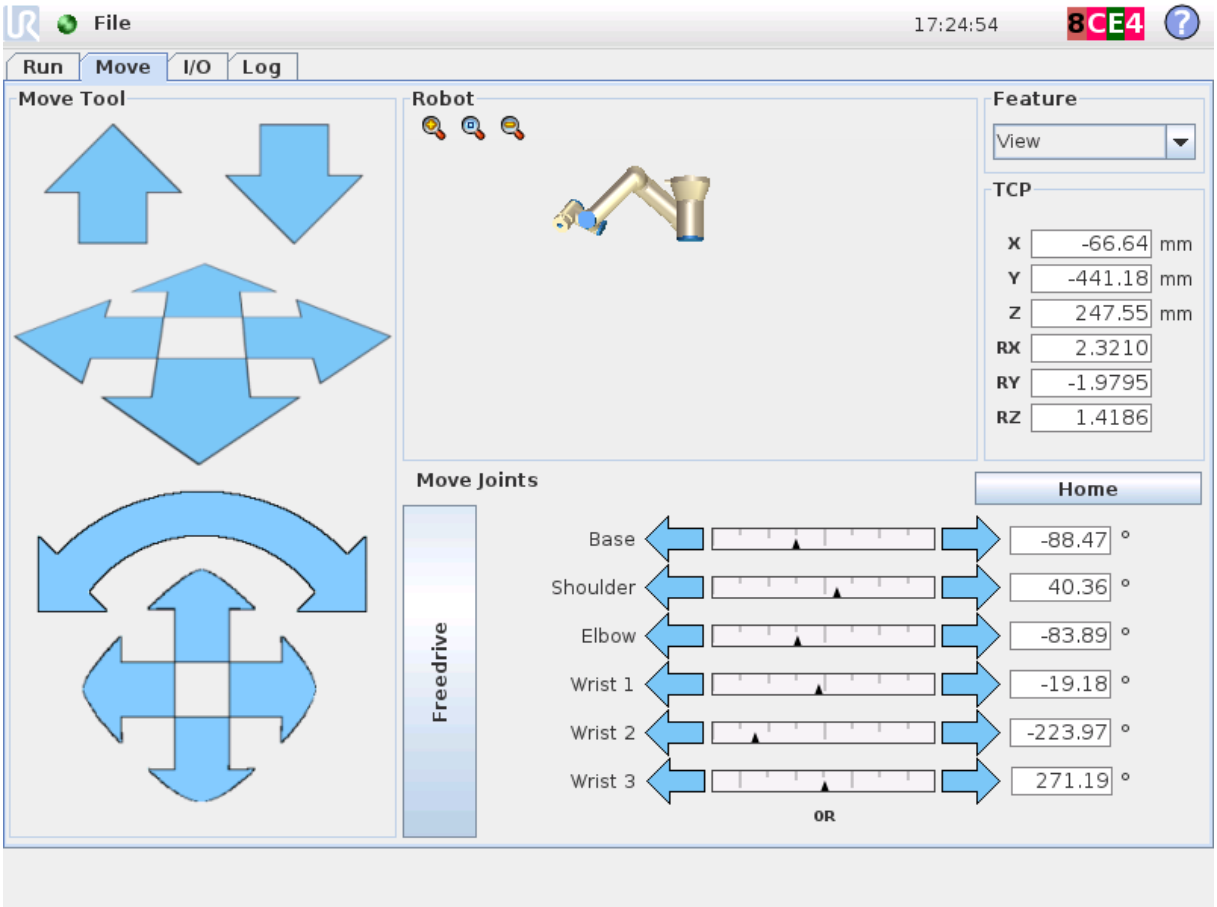

Figure 2.7 Polyscope's interface to move the robot's distal end, as well as each individual joint. A real-time 3D visualization is present and the robot's pose, i.e. position and orientation, is displayed.

Figure 2.8 Polyscope program to move the UR3 robot's distal end during HIFU therapy. The program is started and a 1 mm offset of the UR3s distal end is entered. After pressing the green button, a value for Y and Z can subsequently be entered as well, and robot motion is executed.

2.3.2 Design and implementation of custom robot control software

MATLAB software was used to build a GUI customized for robot and transducer control for atherosclerotic plaque targeting (**Figure 2.9**).

Primarily, any control interface should be able to translate and rotate the UR3 robot in the three orthogonal directions, i.e. x, y and z, separately. Translation of the UR3 robot in these directions was implemented, both in global coordinates, i.e. in the orientation of its Base, and in local coordinates, i.e. in the orientation of the Tool (**Figure 2.10**). By default, the point of rotation is the UR3s end effector. To ensure the transducer stays in place with respect to either the patient's skin, or the last therapy location within the arterial wall, rotation over either the transducer-skin interface or the actual HIFU focus point was implemented (**Figure 2.11**). Rotation over the skin is required prior to HIFU therapy to ensure proper contact of the skin and the bolus cover. Rotating the transducer with respect to the HIFU focus point may be required between subsequent HIFU shots or treatment planes to keep the transducer perpendicular to the target artery.

Utilizing the custom GUI, the robot pose corresponding to the transducer's actual position is displayed real-time and can be saved, along with the axial and lateral HIFU coordinates of each ablation position. Consequently, the transducer can be moved to any of the saved robot poses during HIFU treatment.

If the distance between two subsequent HIFU shots is too large, the created HIFU lesions may not be adjacent. To ensure contiguous lesion formation, the linear distance between subsequent therapy locations are calculated and displayed using the robot poses and corresponding HIFU focus coordinates. 3D lines, representing the robot, the transducer and the HIFU foci, are visualized and expected to improve therapy control throughout a HIFU procedure. All robot motion can be saved and displayed in the GUI, with corresponding times of execution. The number of HIFU shots in the current therapeutic plane is displayed, as well as the number of treated planes and the total number of HIFU shots delivered.

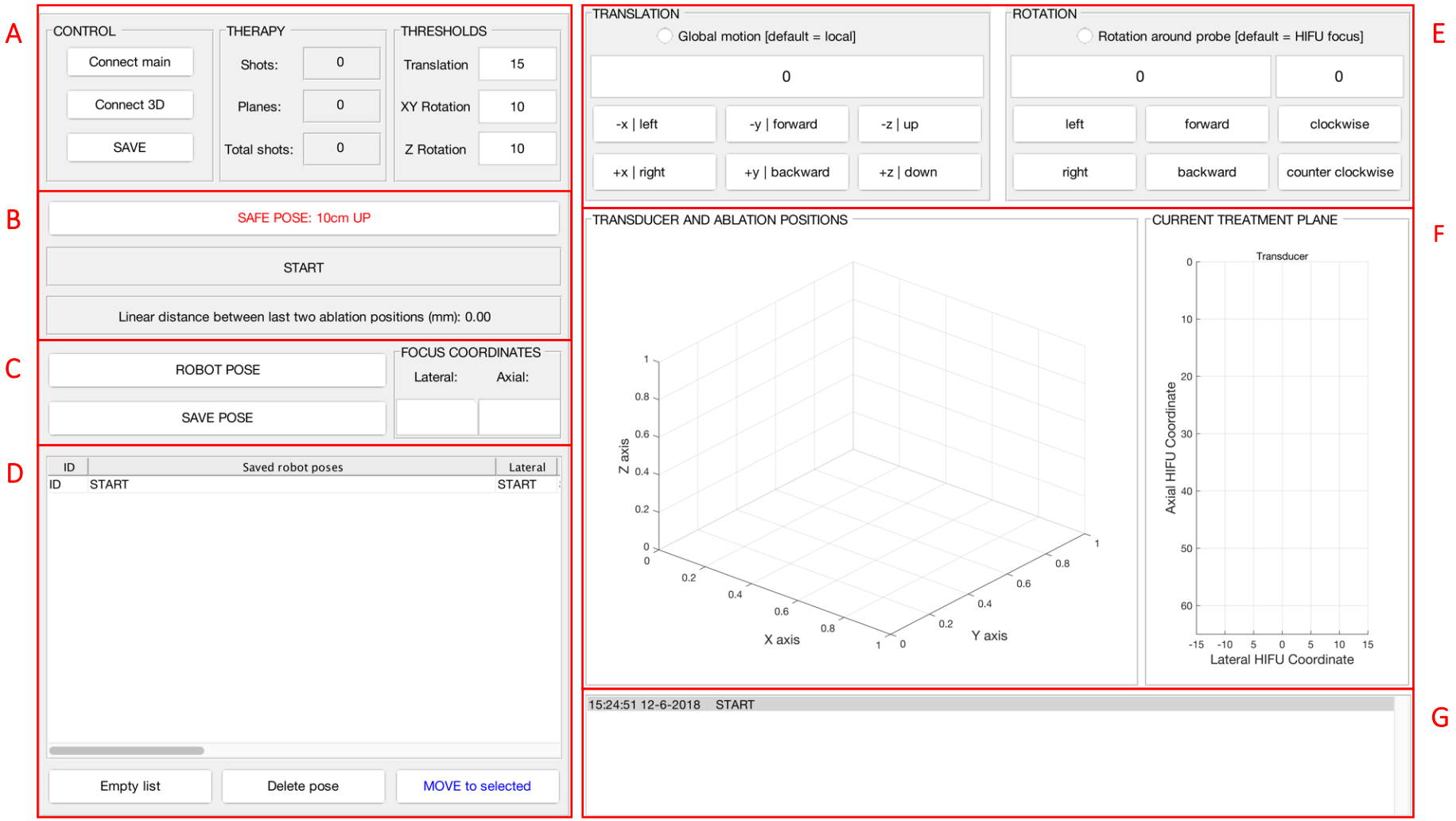

Figure 2.9 Graphical user interface (GUI) designed and built to control and monitor robot motion during a HIFU procedure. **Panel A:** Connect the robot to the GUI or a 3D mouse and save all data, control HIFU shots and treatment planes, and adjust robot motion thresholds. **Panel B:** Move the robot to a safe pose, display the current robot pose and the 3D distance to the previous ablation position. **Panel C:** Display and save the current robot pose with HIFU focus coordinates. **Panel D:** Saved robot poses with HIFU focus coordinates, the robot can be moved to each saved pose. **Panel E:** Execution of robot translations and rotations in x, y and z-direction. The UR3 robot can be translated in the orientation of the Tool (local motion) or the Base (global motion), and rotated around the transducer or the last saved HIFU focus. **Panel F:** Visualization of all 3D transducer and ablation positions, and the 2D ablation positions in the current treatment plane. **Panel G:** Events-file wherein all robot motion is displayed with time and magnitude.

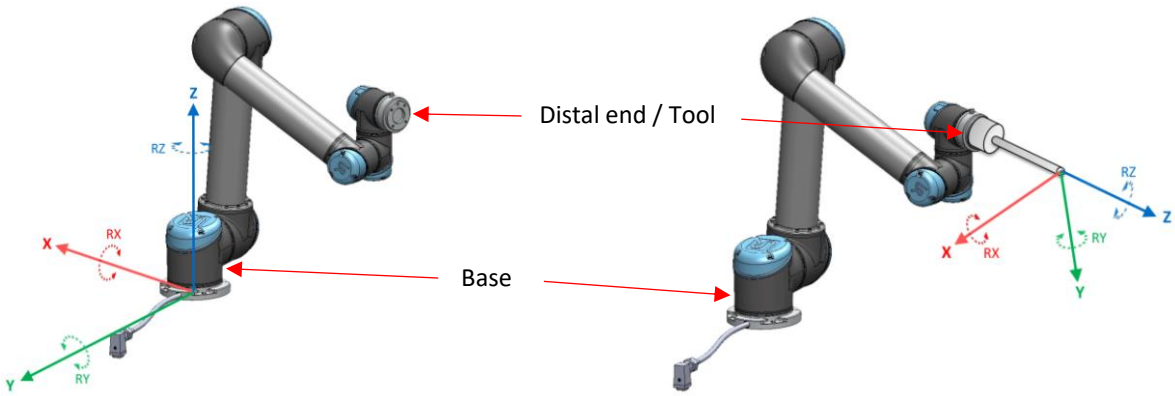

Figure 2.10 UR3 robot translation in direction of, and rotation around the x-axis (red), y-axis (green) and z-axis (blue). **Left.** Translating and rotating the UR3 robot in global coordinates, i.e. in Base orientation. **Right.** Translating and rotating the UR3 robot in local coordinates, i.e. in Tool orientation. Image reproduced from the User Manual (UR3 User Manual, Universal Robotics).

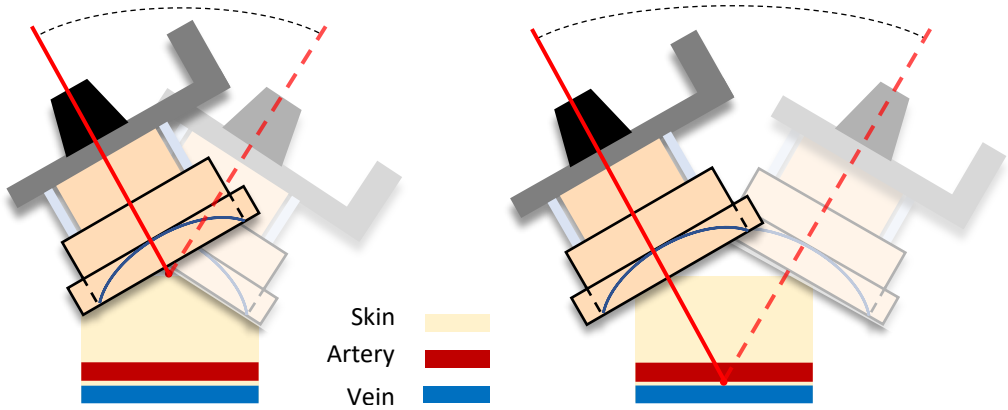

Figure 2.11 Transducer positions prior to rotation (non-transparent) and after rotation (transparent). **Left.** UR3 robot rotation with respect to the transducer-skin interface. **Right.** UR3 robot rotation with respect to the HIFU focus within the arterial wall. HIFU = High Intensity Focused Ultrasound.

2.4 Required accuracy and repeatability of robotic transducer control

As HIFU lesion formation is induced with submillimeter accuracy and to ensure contiguous lesion formation, any potential positioning error should be within the submillimeter range. Repeatability of the UR3 robot is ±0.1 mm[55]. Accuracy of the UR3 robot, i.e. the error between the intended and actual robot motion, is not reported by Universal Robots.

To illustrate, a rotation error of 1.0° at the level of the robot's end effector in one direction, results in a linear 3D positioning error of 1.25 mm at the level of the transducer-skin interface and 1.65 mm at the level of the optimal HIFU focus (**Figure 2.12**). The linear 3D translations at the level of the transducer-skin interface as a result of 0.10, 0.50, 1.00, 2.00 and 5.00-degree rotations at the level of the UR3s end effector are calculated, respectively (**Table 2.1**). Using the custom software, aforementioned translations are calculated in real-time and used to rotate the robot around either the transducer-skin interface or the HIFU focus, instead of the default rotation around the UR3 robot's distal end.

As we aim to deliver HIFU therapy with submillimeter accuracy in subsequent transverse treatment planes spaced 1 mm apart, accuracy and repeatability should be within ±0.1 mm for UR3 robot translations, and ±0.1° for robot rotations. Accuracy and repeatability of robot translations and rotations using the custom software are tested with respect to these requirements (**0**).

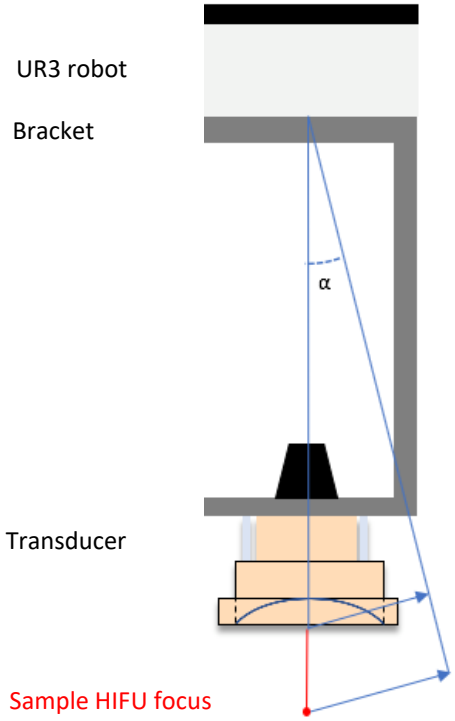

Figure 2.12 Linear displacement of the transducer and the HIFU focus (blue arrows) as a result of rotation around the UR3 robot's distal end with angle α.

Table 2.1 Relationship between a rotation (degrees) at the level of the end effector of the robot, and the resulting linear translation at the transducer-skin interface (mm) and the optimal HIFU focus (mm).

Rotation distal robot end (degrees)	**0.10**	**0.50**	**1.00**	**2.00**	**5.00**
Translation transducer-skin interface (mm)	0.13	0.63	1.26	2.51	6.27
Translation optimal HIFU focus (mm)	0.17	0.83	1.66	3.31	8.26

2.5 Safety measures robotic transducer control

For the entire duration of a HIFU procedure, the transducer will be in direct contact with the patient and exerts continuous pressure on the patient's skin. Additionally, the robot will operate with people and other equipment in its vicinity. For the robotic approach to be safe for patients and therapists, safety measures are required. The robot has multiple safety-related functions (**Table 2.2**) to limit the movement of its joints and the TCP. Additionally, we have implemented several safety-related features in the custom robot control software.

Polyscope

Using Polyscope, the robot's maximum force, power, speed and momentum can be configured such that the robot cannot harm humans or collide with its environment. The maximum power the TCP may exert without harming the patient needs to be investigated, for both the continuous pressure that is performed for the entire duration of a HIFU procedure and for the potential high-energetic impact due to fast or undesired robot motion. Additionally, the maximum joint speed, i.e. the maximum angular velocity of individual joints, and the desired joint position limits, i.e. allowed position range of individual joints, need to be configured accordingly. The position and orientation of the TCP can be limited through the configuration of safety planes and a tool orientation boundary, restricting the operating area of the robot.

Utilizing aforementioned limiting safety functions may improve the safety using our robotic approach. As soon as the robot arm approaches a safety-related limit, the advanced path control software decreases speed or issues a program execution stop. A physical emergency stop button is present which immediately stops robot motion when pressed. Moreover, a Freedrive button is present, which allows the robot to be physically moved when pressed. It is always possible to force a joint to move by pushing or pulling the robot arm hard (500 N). This may be required in case of an emergency or when robot power is either not possible or unwanted.

Table 2.2 Limiting safety-related functions of the UR3 robot, reproduced from[55]. TCP = Tool Center Point robot.

Limiting Safety Function	Description
Joint position	Minimum and maximum angular joint position
Joint speed	Maximum angular joint speed
TCP position	Planes in Cartesian space limiting robot TCP position
TCP speed	Maximum speed of the robot TCP
TCP force	Maximum pushing force of the robot TCP
Momentum	Maximum momentum of the robot arm
Power	Maximum applied robot arm power

Custom software

To limit the risk of unexpected robot motion, translation and rotation thresholds are used in the custom software. These thresholds are defined to prevent excessive pressure on the patient and collision with other people or additional equipment. Translations exceeding 15 mm and rotations exceeding 10° need to be confirmed with an additional check, prior to robot execution. If necessary, these thresholds can be adjusted in the GUI. In case of excessive pressure or if immediate access to the treatment site is required, the robot needs to be moved away quickly. A safe button is implemented in the software, which immediately moves the robot 100 mm upwards in global coordinates, i.e. away from the patient (**Figure 2.9** and **Figure 2.10**).

2.6 Conclusion

The experimental setup to target atherosclerotic plaques with HIFU incorporates a HIFU system, a DMUA-transducer and an industrial six-DOF UR3 robot. The DMUA-transducer and the robot are integrated using a customized steel frame and bracket. A water degassing system and bolus cover facilitate circulation of degassed water through the bolus, and thereby US coupling to the region of interest.

As using Polyscope for localization, targeting and monitoring during a HIFU procedure was rather laborious, custom robot control software was designed and implemented investigated. A custom GUI was designed and implemented to improve robot control (**Table 2.3**). The GUI is expected to improve transducer positioning and monitoring with the real-time visualization of the 3D ablation positions, displaying the distance between subsequent ablation positions, and the possibility to save each therapeutic robot position.

Multiple software-related safety measures were applied in both Polyscope and the custom software, and the required accuracy and repeatability of using the UR3 and the custom software for atherosclerotic plaque targeting were defined (**Table 2.4** and **Table 2.5**). To ensure contiguous lesion formation and sufficient monitoring during a HIFU procedure, these requirements need to be tested using the custom software and experimental setup (**0**).

Table 2.3 Functionalities of custom designed and implemented graphical user interface for UR3 robot control.

Facilitate external control of the UR3 robot in Polyscope
1. Receive robot poses through Ethernet connection
2. Send robot command with desired robot pose through Ethernet connection

Robot control utilizing the custom MATLAB-software
1. Connect and disconnect to / from robot
2. Receive and save robot poses with axial and lateral HIFU coordinates
3. Calculate desired robot poses
a. Facilitate submillimeter displacements of the transducer
b. Translate robot in global and local coordinates
c. Rotate transducer around transducer-skin interface and HIFU-focus
4. Move to saved robot poses
a. 3D visualization of the UR3s TCP, the transducer, and the HIFU-foci
b. Log all robot motion
c. 3D mouse control of the UR3 robot

Table 2.4 Software-related safety measures in the graphical user interface and Polyscope.

Safety measures custom software		
1.	Translation threshold	15 mm
2.	Rotation threshold	10°
3.	Safe pose	100 mm up in global coordinates

Safety measures UR3 robot			
1.	General limits	**Maximal**	**Normal mode**
	a. Force (N)	250	150
	b. Power (W)	1000	300
	c. Speed (mm/s)	5000	1500
	d. Momentum (kg m/s)	100	25
2.	Joint limits		
	a. Joint speed	191°/s	
	b. Joint position	-363° to 363°	
3.	Boundaries		
	a. Safety planes TCP position	Not configured	
	b. Tool orientation boundary TCP	Not configured	
4.	Safety inputs and outputs	Not configured	

Table 2.5 Accuracy and repeatability requirements of UR3 robot control.

Requirements UR3 robot control		
1.	Repeatability	±0.1 mm
2.	Accuracy translations	±0.1 mm
3.	Accuracy rotations	±0.1°

Chapter 3 Requirements of robotic transducer control

3.1 Introduction

During HIFU therapy, the transducer is moved between ablation positions, imaging is performed to verify proper positioning and subsequently HIFU therapy is delivered. Utilizing the custom software, ablation positions can be saved, visualized and used to return the transducer to specific therapy locations during a HIFU procedure. To ensure contiguous lesion formation, we investigated the previously discussed requirements with respect to 1) robot accuracy and 2) repeatability, for different functionalities of the custom software and Polyscope (**Table 3.1**). To guarantee safe use of the robot we investigated 1) the expected force and impact of the robot's distal end (the tool), 2) motion of the UR3s distal end in case of an emergency break, and 3) the applied robot force by the UR3s distal end in case of an emergency break.

Table 3.1 Accuracy and repeatability requirements of UR3 robot control.

Test	Required	Universal robots
1. UR3 translation accuracy	±0.1 mm	Not reported
d. Translation accuracy using the custom software. e. Translation accuracy under pressure. f. Translation accuracy using Polyscope.		
2. UR3 rotation accuracy	±0.1 mm	Not reported
a. Accuracy of rotation angles using the custom software b. Accuracy of rotating the UR3 around a saved HIFU focus using the custom software.		
2. UR3 repeatability	±0.1°	±0.1 mm
a. Repeatability of translations using the custom software b. Repeatability of returning the UR3 to saved robot poses using the custom software.		

3.2 Materials and Methods

3.2.1 Translation accuracy

Translation accuracy using the custom software

To measure the accuracy of robot motion using the custom software, the UR3 robot's distal end was placed against a digital measuring device, which was calibrated to zero prior to moving the robot. Robot motion in the direction of the measurement device was performed, ten times for each distance. For 0.15, 0.25, 0.5, 1, 2, 5 and 10 mm translations an electronic digital indicator (Mitutoyo Digimatic Indicator, Mitutoyo, Japan) with 0.001 mm accuracy was used to measure the distance over which the tool moved (**Figure 3.1**.**A**). For 20, 50 and 100 mm translations, a digital caliper (Mitutoyo Absolute Digimatic Caliper, Mitutoyo, Japan) with 0.01 mm accuracy was used (**Figure 3.1.B**).

For all robot experiments, the measurements were subtracted from the intended distances or rotations, and the mean, standard deviation and range were calculated for the error of each distance or rotation using MATLAB (MathWorks, Inc., Natick, MA, USA).

Translation accuracy under pressure

For 1, 2, 5 and 10 mm translations, the previous experiment was repeated ten times with the robot's distal end exerting a downwards force of approximately 50 N against a force gauge (Advanced Force Gauge 1000N, Mecmesin, Slinfold, West Sussex, UK). The force gauge has an accuracy of 1 Newton (N) and a 5 kHz sample rate (**Figure 3.2**.**A**).

Translation accuracy using Polyscope

Using Polyscope, the UR3s distal end was moved 1, 2, 5 and 10 mm in direction of the digital indicator, respectively (**Figure 3.1.A**). The experiment was repeated ten times for each distance.

Agreement between robot control through Polyscope and the custom software for 1 mm translations was assessed by calculation of the Bland-Altman 95% limits of agreement using SPSS Statistics Version 24 (SPSS, Chicago, IL, USA).

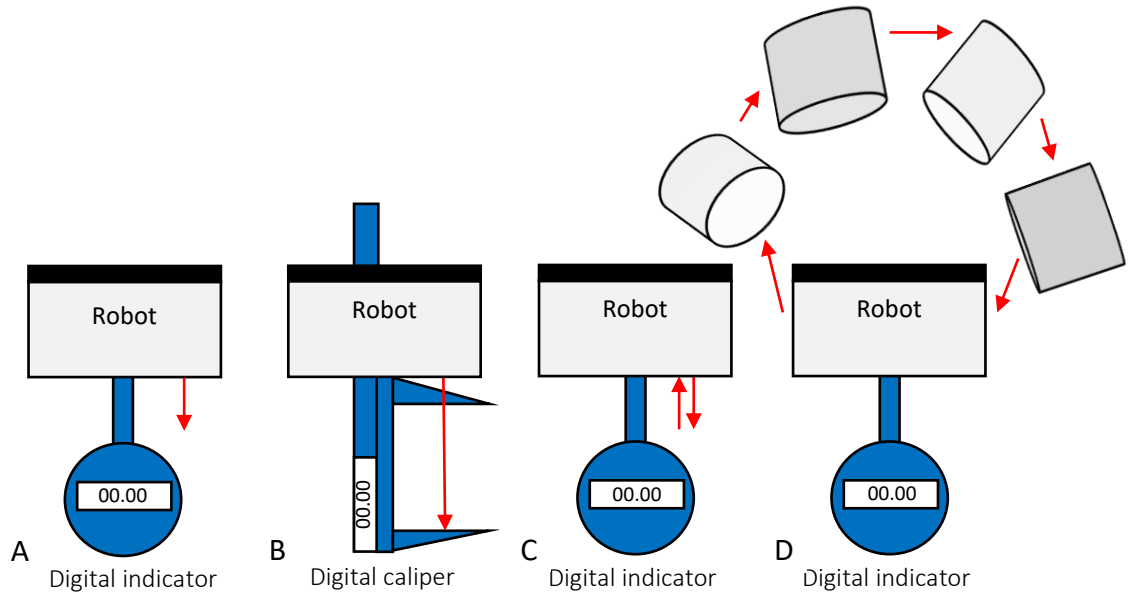

Figure 3.1 Robot motion (red arrows) during the accuracy and repeatability experiments using the custom software. **A:** UR3 robot accuracy. **B:** UR3 robot accuracy. **C:** UR3 robot repeatability. **D:** UR3 robot repeatability saved poses.

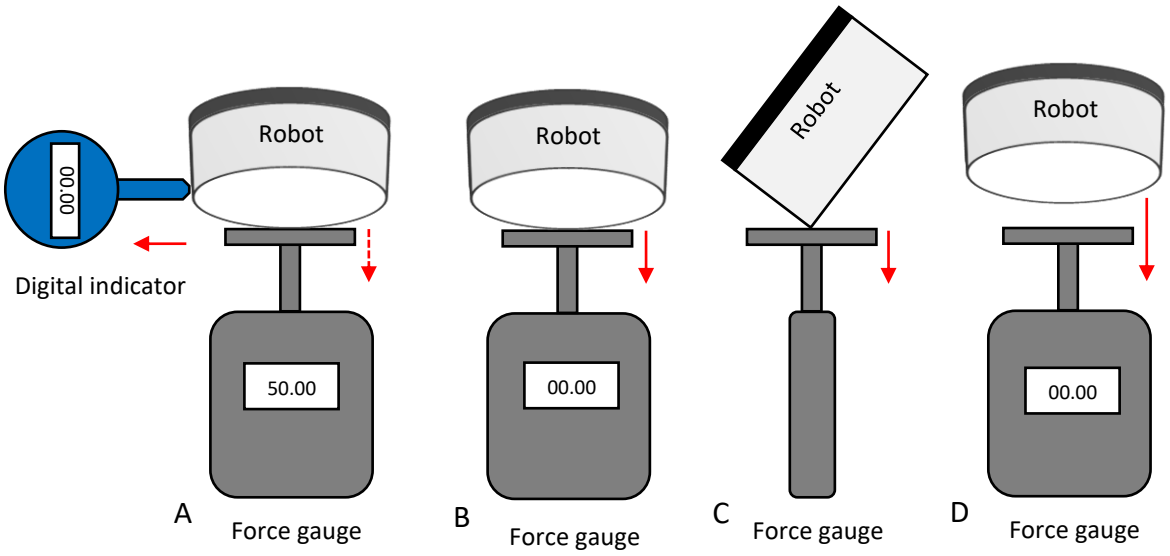

Figure 3.2 Robot motion (red arrows) during the force and impact measurements. **A:** Maximum tool force measurements for 1 mm translations and during an emergency break. **B:** Maximum tool impact with varying distance and speed. **C:** Side view of the UR3s distal end against the power gauge. **D:** UR3 robot accuracy under pressure.

3.2.2 Rotation accuracy

Accuracy of rotation angles using the custom software

To measure the accuracy of UR3 robot rotations, a digital distance laser (Bosch Professional GLM 30, Bosch GmbH, Germany) with 2 mm accuracy was horizontally attached to the distal end of the robot in direction of the x, y, and z-rotations of the tool, i.e. forward-backward, left-right, and (counter)clockwise rotations, respectively. Cardboard was placed against the facing wall and the distance to the cardboard was measured using the laser. The distance between the point of rotation, i.e. the center point of the UR3s distal end, and the cardboard varied for each rotation direction (x, y and z), depending on the specific robot configuration and laser mounting.

Prior to each rotation, the robot was moved to the saved pose with the laser positioned horizontally. The laser was subsequently used to visualize the tool orientation on the cardboard before and after 1, 2, 5 and 10° rotations in the x, y and z-direction, respectively (**Figure 2.10** and **Figure 3.3**). For each rotation, the laser beam was marked in the cardboard with a needle. Finally, the cardboard was placed horizontally with the laser positioned at point C, and the distance to a wooden stave, positioned at the level of point B, was measured (**Figure 3.3**). The angle of rotation was calculated using the horizontal distance between the laser and the facing wall, and the measured distances before and after rotation (**Equation 3.1**). Each rotation was measured ten times.

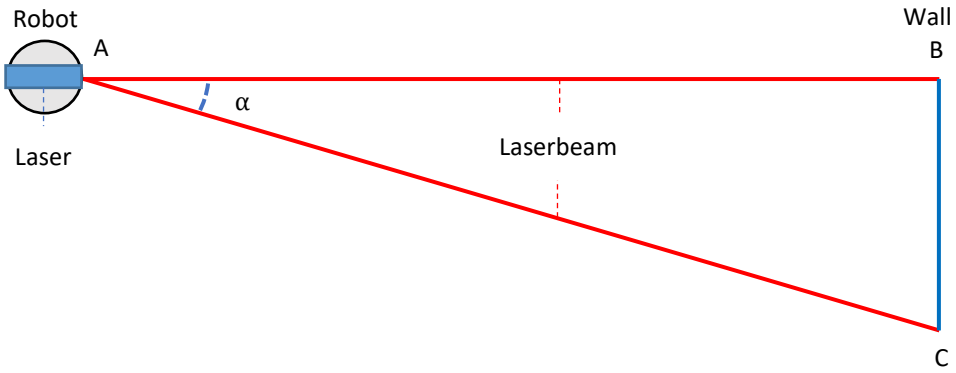

Figure 3.3 UR3 robot rotation accuracy experiments using the custom software. A digital distance laser is attached horizontally to the distal end of the robot (A). The end of the laser beam was marked on the cardboard before (B) and after (C) rotation. The distances AB and BC were measured and used to calculate the angle of rotation (α).

$$\alpha = \boldsymbol{tan}^{-1}\left(\frac{\boldsymbol{BC}}{\boldsymbol{AB}}\right)$$

Equation 3.1

Accuracy of rotating the UR3 around a saved HIFU focus

The accuracy of rotating the UR3 around a saved HIFU ablation position was investigated with the digital distance laser vertically attached to the UR3s distal end, facing down. A wooden stave was horizontally fixed to a table, and the UR3 was positioned above the wooden beam. Using the custom software, the robot pose was saved with the distance between the laser and wooden beam as axial HIFU coordinate. This distance is used by the software to calculate the required robot translation to rotate around a HIFU focus. A needle was used to mark the laser in the wooden stave before and after robot rotation. Subsequently, the distance between the two points was measured using a digital caliper. The experiment was repeated ten times, for 20-degree rotations in the x and y rotation direction, respectively. As z-rotations are not required to rotate around a saved HIFU focus during therapy, this direction was not measured.

3.2.3 Repeatability

Repeatability of robot translations using the custom software

The UR3 was positioned with its distal end pressing against the electronic digital indicator, which was then calibrated to zero. Repeatability of linear translations was tested by moving the tool 10, 20, 50 or 100 mm away from the indicator and back (**Figure 3.1.C**).

Repeatability returning to saved robot poses

Repeatability of returning the UR3 to saved robot poses was tested by moving the robot to four randomly saved poses, and back to its original pose against the digital indicator (**Figure 3.1.D**). The distance on the digital indicator upon return represents the positioning error before and after robot motion. Both experiments are repeated ten times for each distance and set of robot poses, respectively.

3.2.4 UR3 tool force

The robot power at the UR3s distal end cannot be directly translated to the configured maximum robot power configured in Polyscope, as this depends on the impact and acceleration of the robot, and the power required by the individual robot joints. Additionally, Universal Robots does not provide information on the underlying algorithms and these factors vary with each robot configuration. To measure the maximum robot power that is expected to be applied during a typical HIFU procedure, the robot power at its distal end was measured using the saved robot poses of the first nine animal experiments (**0**).

The UR3 was moved to the saved robot pose corresponding to the last therapy location of each animal experiment using Polyscope. The steel frame with the robot was moved to position the robot's inferior part of the distal end against the power gauge, which was subsequently calibrated to zero (**Figure 3.2.B** and **Figure 3.2.C**). The robot pose was saved in the GUI and the UR3 was moved 1 mm in direction of the power gauge in

tool orientation. This was repeated until a protective stop was induced by the robot to measure the maximum exerted force using the *Maximum Hold* function of the power gauge. After restarting the UR3, it was moved back to the saved pose. This experiment was repeated ten times and the mean, range and standard deviation were calculated.

3.2.5 UR3 tool impact force

To measure the potential maximum impact force of the tool during the performed animal experiments the UR3 was moved to the therapy pose wherein the measured force was highest, i.e. to the third 14-days follow-up animal experiment (**Table 3.7**).

The UR3 was positioned 10 mm above the force gauge, which was subsequently calibrated to zero. The tool speed was 0.2 mm/s and the acceleration was 0.02 mm/s^2, similar to the speed and acceleration used during the animal experiments. The robot was moved 20 mm downwards in global coordinates and the maximum force due to the impact of the distal robot end was measured while a protective robot stop occurred (**Figure 3.2.D**). The experiment was repeated ten times, and repeated for a tenfold of the tool speed and acceleration, i.e. 2 mm/s and 0.2 mm/s^2, respectively.

3.2.6 Motion and applied force in case of an emergency break

Linear 3D motion during an emergency break and upon robot restart

The UR3 was positioned with its distal end pressing against the electronic digital indicator, which was then calibrated to zero (**Figure 3.2.B** and **Figure 3.2.C**). The robot pose was saved using the custom software, and the emergency button on the Touchpad was pressed. The offset was measured immediately after the emergency stop, after restarting the UR3, and upon return to the original saved robot pose, respectively. This was repeated ten times.

Exerted force during an emergency break and upon robot restart

The UR3 was moved to a saved robot pose corresponding to the last therapy location of each animal experiment using Polyscope (**0**). The steel frame with the robot was moved to position the inferior part of the UR3s distal end against the power gauge, which was subsequently calibrated to zero (**Figure 3.2.B** and **Figure 3.2.C**). The robot pose was saved in the GUI, and the emergency button on the Touchpad was pressed. The maximum force exerted onto the power gauge during the emergency break and upon robot restart were measured, respectively. The UR3 was subsequently restarted and moved back to the saved pose. This experiment was repeated ten times for the last saved robot pose of each of the nine animal experiments. The mean, range and standard deviation was calculated for the applied robot force.

3.3 Results

3.3.1 Translation accuracy

Translation accuracy using the custom software

The mean error of robot positioning with the custom software remained under ±0.1 mm for all translations (**Table 3.2** and **Figure 3.5**).

Translation accuracy using the custom software with force at the UR3s distal end

The mean translation accuracy with 50 ±2 N exerted by the robot's distal end was below ±0.1 mm for 1 and 2 mm translations, and higher than 0.1 mm for 5 and 10 mm translations (**Table 3.3**).

Translation accuracy using Polyscope

The mean accuracy of 1 to 10 mm translations using Polyscope was below ±0.1 mm (**Table 3.2**). No significant differences between Polyscope and the custom software were found as measurements are inside the Bland-Altman 95% limits of agreement (**Figure 3.4**). The mean difference between 1 mm robot motion using Polyscope and the custom software was 0.0115 ±0.02172 mm.

Table 3.2 Mean translation errors with standard deviation and range.

Distance (mm)	Custom software (mm)	Using Polyscope (mm)
0.15	0.0063 ±0.0204 [-0.0280 – 0.0410]	
0.25	-0.0052 ±0.0151 [-0.0340 – 0.0170]	
0.5	-0.0027 ±0.0142 [-0.0240 – 0.0190]	
1	0.0029 ±0.0144 [-0.0320 – 0.0220]	0.0088 ±0.0288 [-0.0360 – 0.0580]
2	-0.0133 ±0.0086 [-0.0270 – 0.0020]	0.0078 ±0.0316 [-0.0380 – 0.0750]
5	-0.0272 ±0.0114 [-0.0440 – -0.0090]	0.0252 ±0.0528 [-0.0530 – 0.0950]
10	-0.0512 ±0.0066 [-0.0620 – -0.0400]	0.0685 ±0.0135 [0.0440 – 0.0870]
20	0.0060 ±0.0667 [-0.1000 – 0.0900]	
50	0.0310 ±0.0802 [-0.0600 – 0.1500]	
100	0.0370 ±0.0250 [-0.0100 – 0.0800]	

Table 3.3 Mean translation error using Polyscope and when force is exerted by the UR3s distal end, with standard deviation and range.

Distance (mm)	Accuracy under pressure (mm)
1	0.0457 ±0.0253 [-0.0070 – 0.0770]
2	0.0394 ±0.2870 [0.0060 – 0.0920]
5	0.1014 ±0.0491[0.0250 – 0.1980]
10	0.2822 ±0.0456 [0.1970 – 0.3390]

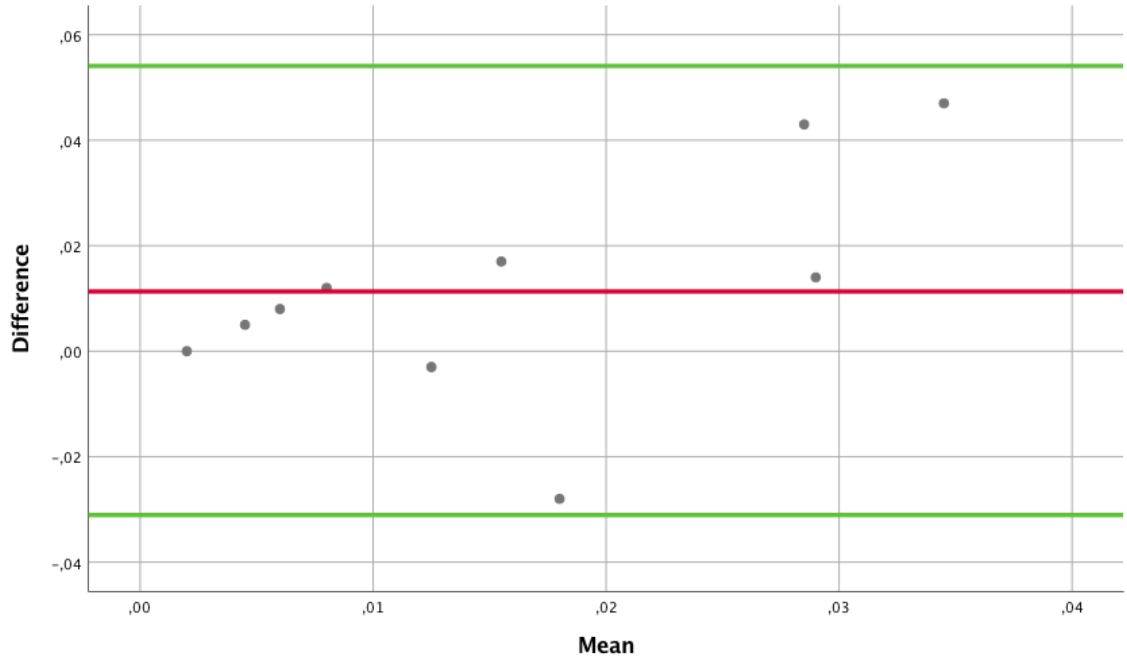

Figure 3.4 Bland-Altman plot of 1 mm translation accuracy using Polyscope and the custom software. Mean is visualized (red line), along with 95% limits of agreement (green lines).

3.3.2 Rotation accuracy

Rotation accuracy: accuracy of rotation angles using the custom software

The measured distances were used to calculate the distance between the point of rotation of the UR3s distal end and the cardboard, depending on the specific robot configuration and laser mounting (**Table 3.4**). The mean error of robot positioning remained under ±0.1° for rotations in all three directions (**Table 3.5**and **Figure 3.6**).

Rotation accuracy: rotating the UR3 around a saved HIFU focus

Accuracy of rotating the UR3 around a saved HIFU focus in the x and y-direction was 0.7880 ±0.1971 mm (range 0.5 – 1.1 mm) and 0.5550 ± 0.1854 mm (range 0.24 – 0.80 mm), respectively.

Table 3.4 Distances between the point of rotation and the cardboard for each rotation direction and magnitude.

Direction / **Magnitude**	**Distance X (mm)** (forward-backward)	**Distance Y (mm)** (left-right)	**Distance Z (mm)** (counter-clockwise)
1°	9359	9520	9614
2°	9355	9516	9614
5°	9311	9513	9614
10°	9285	9510	9614

Table 3.5 Mean rotation error in the x, y and z-direction with standard deviation and range.

Rotation (degrees)	Mean error X (degrees)	Mean error Y (degrees)	Mean error Z (degrees)
1	-0.0112 ±0.0115	0.0239 ±0.0062	0.003 ±0.0124
Range	[-0.0345 – 0.0083]	[0.0191– 0.0371]	[-0.0190 – 0.0617]
2	-0.0032 ±0.0095	0.0048 ±0.0086	0.0186 ±0.0057
Range	[-0.0142 – 0.0164]	[-0.0042 – 0.0199]	[0.0072 – 0.0280]
5	-0.0036 ±0.0063	0.0202 ±0.0066	0.0566 ±0.0050
Range	[-0.0146 – 0.0037]	[0.0136 – 0.0316]	[0.0477 – 0.0655]
10	0.0431 ±0.0069	0.0852 ±0.0068	0.0562 ±0.0062
Range	[0.0311 – 0.0550]	[0.0752 – 0.0928]	[0.0469 – 0.0701]

3.3.3 Repeatability

The mean error between the original and saved robot pose upon return was -0.0118 ±0.0174 mm (range -0.0320 – 0.0250 mm). The mean error of robot repeatability remained under ±0.1 mm for all translations and for returning the robot to a saved robot pose (**Table 3.6** and **Figure 3.5**).

3.3.4 UR3 tool force

For each robot pose, the maximum power exerted by the robot's distal end was measured, and the range and standard deviation was calculated (**Table 3.7**). The maximum measured force was 105.9 N, corresponding to the last saved robot pose of the third 14-days follow-up animal experiment. The lowest force measured was 70.6 N, measured for the last saved robot pose of the first acute animal experiment. Standard deviation varied from 0.4 to 1.4 N for all poses.

3.3.5 UR3 tool impact force

The maximum measured force during tool impact was 114.7 N, measured after 10 mm motion with 2.0 mm/s and an acceleration of 0.2 mm/s^2 (**Table 3.8**). The lowest force measured was 94.6 N, measured after 100 mm motion with 0.2 mm/s and an acceleration of 0.02 mm/s^2.

Table 3.6 Mean translation error upon return after backwards and forward translations with standard deviation and range.

Distance (mm)	Mean translation error (mm)
10	-0.0025 ±0.0043 [-0.0130 – 0.0010]
20	0.0110 ±0.0094 [-0.0060 – 0.0230]
50	0.0087 ±0.0058 [-0.0030 – 0.0170]
100	-0.0039 ±-0.0053 [-0.0140 – 0.0030]

Table 3.7 Means of the maximum tool forces measured before the occurrence of a protective robot stop for the last robot pose of the preclinical animal experiments, with standard deviation and range.

Animal experiment pose	Mean force at UR3s distal end (N)
Acute 1	70.6 ±0.6 [69.6 – 71.2]
Acute 2	81.7 ±0.4 [80.8 – 82.2]
Acute 3	105 ±0.8 [103.8 – 106.4]
3-days follow-up 1	96.3 ±1.4 [94.4 – 97.8]
3-days follow-up 2	80.6 ±0.6 [80.0 – 81.2]
3-days follow-up 3	100.6 ±0.6 [99.6 – 101.6]
14-days follow-up 1	75.5 ±0.5 [74.8 – 76.2]
14-days follow-up 2	99.8 ±1.0 [97.4 – 101.2]
14-days follow-up 3	105.9 ±0.9 [103.8 – 106.8]

3.3.6 Motion and applied force in case of an emergency break

Linear motion during an emergency break and upon robot restart

The mean 3D robot position deviations immediately after an emergency break, after restarting the robot, and after returning to the saved position, were 3.0289 ±0.7751 mm (range 1.1870 – 3.9090 mm), 3.4541 ±0.0562 mm (range 3.3170 – 3.5080 mm), and 0.0010 ±0.1211 mm (range -0.0270 – 0.0150), respectively (**Figure 3.5**). Highest mean robot position deviation was 3.4541 mm, measured upon robot restart. The mean positioning error after an emergency break was below 0.1 mm upon return to the last saved robot pose (**Figure 3.5**).

Exerted force during an emergency break and upon robot restart

The maximum measured force at the robot's distal end after an emergency break and upon robot restart was 30.2 N and 76.1 N, respectively (**Table 3.9**). As aforementioned, the distal robot end is stabilized by its internal motors, which causes the robot joints and distal end to move upon restarting the UR3. In four out of nine robot poses, the distal end did not move towards the power gauge after pressing the emergency button.

Table 3.8 Maximum tool force for varying distances, speed and acceleration, with standard deviation and range.

Distance to gauge (mm)	Speed (mm/s)	Acceleration (mm/s^2)	Maximum force (N)
10	0.2	0.02	109.6 ±1.1 [108.0 – 111.4]
10	2.0	0.20	114.7 ±1.0 [113.2 – 116.6]
100	0.2	0.02	94.6 ±0.3 [94.4 – 95.2]
100	2.0	0.20	96.9 ±0.5 [96.2 – 97.8]

Table 3.9 Mean of the maximum tool forces measured immediately after pressing the emergency button and upon robot restart, with standard deviation and range.

Animal experiment pose	After emergency break (N)	Upon robot restart (N)
Acute 1	25.4 ±0.7 [24.4 – 26.8]	43.2 ±1.9 [38.6 – 45.4]
Acute 2	26.3 ±0.5 [25.6 – 27.0]	69.9 ±0.7 [68.8 – 71.0]
Acute 3	21.2 ±1.5 [18.8 – 23.2]	*Not in direction of gauge*
3-days follow-up 1	30.2 ±0.4 [29.8 – 31.0]	75.5 ±1.0 [74.2 – 76.8]
3-days follow-up 2	29.5 ±1.0 [28.0 – 31.0]	76.1 ±0.3 [75.6 – 76.6]
3-days follow-up 3	23.4 ±1.8 [20.8 – 25.4]	*Not in direction of gauge*
14-days follow-up 1	15.6 ±0.8 [14.8 – 17.2]	*Not in direction of gauge*
14-days follow-up 2	21.9 ±0.5 [21.0 – 22.6]	*Not in direction of gauge*
14-days follow-up 3	20.6 ±0.4 [20.0 – 21.2]	39.0 ±0.6 [38.4 – 40.2]

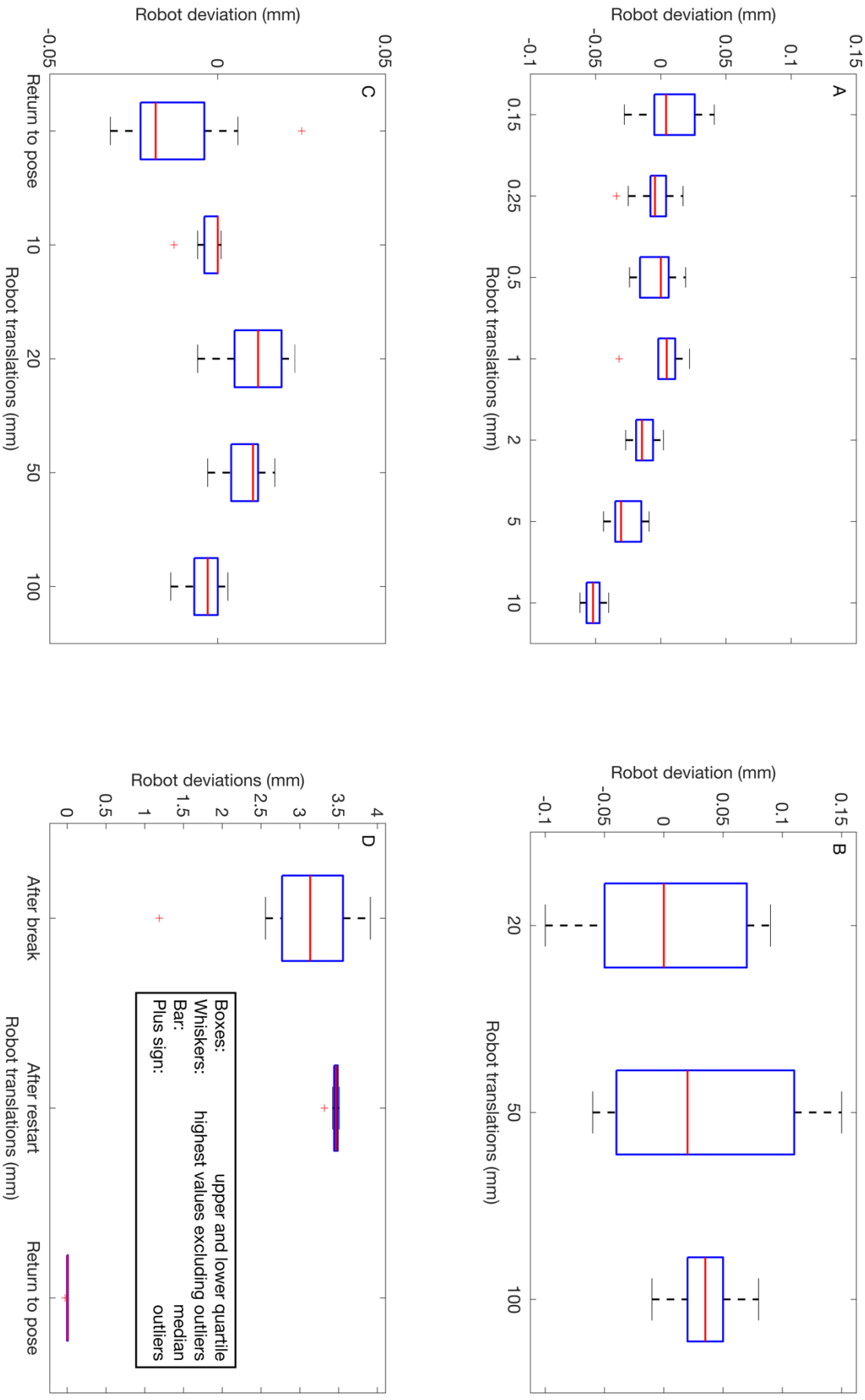

Figure 3.5 Robot accuracy and repeatability using the custom software. **A:** Robot accuracy for 0.15 – 10 mm translations. **B:** Robot accuracy for 20 – 100 mm translations. **C:** Robot repeatability upon return to a saved robot poses, and after 10 – 100 mm translations. **D:** Robot motion and accuracy in case of an emergency break.

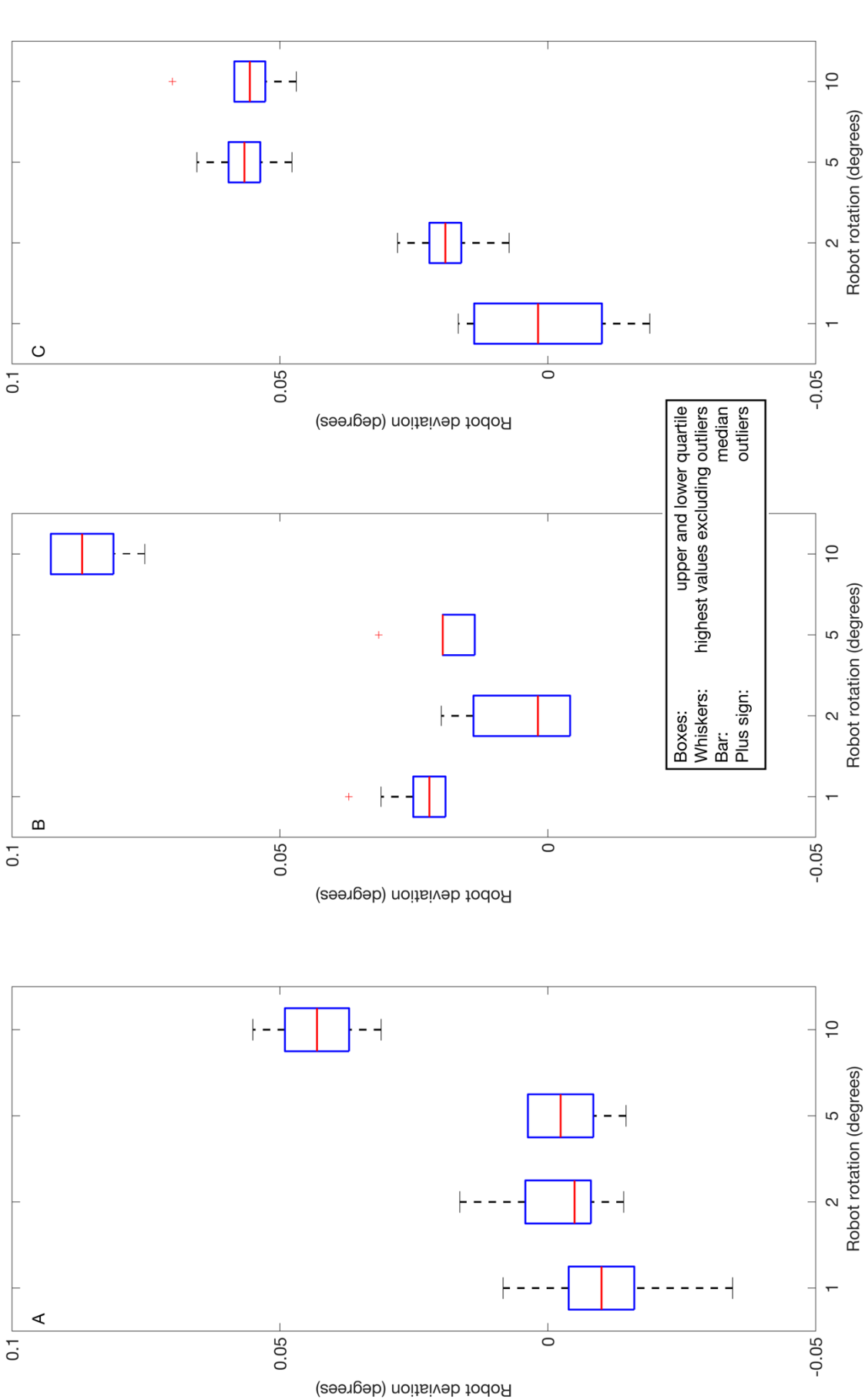

Figure 3.6 Accuracy of robot rotations using the custom software. **A.** Robot accuracy forward-backward rotations (X). **B.** Robot accuracy left-right rotations (Y). **C.** Robot accuracy (counter)clockwise rotations (Z).

3.4 Discussion

We have tested the accuracy and repeatability of controlling the UR3 with the custom software with respect to the previously defined requirements (**Table 3.1**).

The mean positioning error was below ±0.1 mm for all translations and for the repeatability, which is in line with the repeatability of ±0.1 mm as stated by Universal Robots. The positioning error was smaller than ±0.1 mm for robot translations using Polyscope, as well as for returning the UR3 robot to saved robot poses using the custom software. Additionally, robot control using the custom software and using Polyscope were compared for 1 mm translations and no significant differences were found.

Accuracy and repeatability of the robot and the custom software were tested for commonly used distances during the application of HIFU therapy. During initial positioning, the DMUA-transducer is moved over relatively large distances to verify proper positioning with respect to target tissue, typically between 25 and 40 mm parallel to the target artery. Subsequently, the transducer is moved upwards and downwards, to verify proper positioning on diagnostic US, or to apply more US gel. Relatively small robot rotations are performed between subsequent HIFU shots, to maintain perpendicularity of the transducer with respect to the target area. Although the use of larger rotations is limited, it may be useful to test the accuracy of larger rotations in the future.

The mean rotation error was smaller than ±0.1° for robot rotations in all three directions. The angles of rotation were calculated using goniometric function (the tangent), assuming a straight 90° angle between the laser beam and the facing wall, while we cannot be sure that the floor and the opposite wall are perfectly straight and perpendicular to one another. These potential positioning inaccuracies may have affected the calculated rotation errors.

20-degree rotations around a saved HIFU focus resulted in a mean linear positioning error of 0.8 and 0.6 mm for the x and y-direction, respectively. As the distance between the laser and the wooden stave was relatively small, i.e. between 500 and 600 mm, the size of the laser beam was relatively large compared to the size of the compass needle. It was therefore difficult to mark the linear differences before and after robot rotation, relative to the laser beam. Additionally, the linear differences between the laser beam before and after robot rotation were measured on a 2D surface, while rotations were performed in 3D. Any upward or downward motion of the UR3s distal end as a result of 3D robot rotation was therefore not included in the measurements. We tried to compensate for this limitation by rotating the UR3 over its center position above the wooden stave, from a -10° rotation on one side, to a 10° rotation position on the other side, for both the x and y-direction. However, it is hypothesized that aforementioned limitations resulted in overestimated rotation errors. Positioning errors during 3D rotations over a HIFU focus point may need to be better quantified in the future, for example by using an ultrasound phantom containing visible markers with predefined distances to simulate HIFU treatment.

When a force was exerted by the UR3s distal end, 5 and 10 mm translations resulted in a positioning error of 0.1 and 0.3 mm, respectively. It was difficult to position the digital indicator horizontally at the same height as the

URs distal end, and exactly in line with the executed robot translations. We hypothesize that the measured errors were overestimated due to these positioning inaccuracies.

The highest tool force measured was 105.9 N, corresponding to the last saved robot pose of the third 14-days follow-up animal experiment. Highest tool force measured during tool impact was 114.7 N for 2.0 mm/s and an acceleration of 0.2 mm/s^2. The highest mean tool offset after an emergency break was 3.5 mm, measured upon robot restart after an emergency break. As relatively large distances were used to push the transducer onto the skin during the first animal experiments, i.e. up to 20 mm, 3.5 mm robot motion in case of an emergency break is not expected to harm the patient.

Highest tool force exerted after an emergency break was 76.1 N, also measured upon robot restart. As observed in the force measurements, the robot's distal end did not always move in direction of the power gauge after an emergency break, and thus not towards a hypothetical patient. The robot moved either in direction of the power gauge or in the opposite direction, away from the power gauge. The positioning error was below $\pm$0.1 mm upon return to the last saved robot pose using the custom software.

Based on preliminary testing, tool speed was lowered to 0.2 mm/s, and the angular joint position and speed were not restricted to maintain sufficient speed of robot motion during a HIFU experiment. As the configuration of the robot varies for each procedure, depending on the operating room and location of the target, we did not implement safety planes to limit the robots Tool Center Point (TCP) position. Ideally, these planes are defined prior to each individual HIFU procedure, limiting the robot to move outside the target area. Doing so may minimize the risk of robot collision with humans and equipment in its environment. In the future, it may be useful to investigate if the required time for safety plane configurations prior to HIFU treatment is feasible in daily clinical practice.

3.5 Conclusion

In this study, we find that the robot translations and most rotations can be executed with the desired accuracy and repeatability using the custom software. Returning the UR3 to saved therapy positions throughout HIFU treatment and after an emergency break was also found to be within the desired accuracy. Accuracy of rotating the transducer around a HIFU focus point can be better quantified in the future. The exerted force by the UR3 at the level of the transducer-skin interface depends on the specific robot configuration. To minimize the risk of undesired robot motion in the future, the feasibility of configuring safety planes prior to HIFU treatment may need to be investigated.

One study that investigated the integration of US imaging-guidance and robotic positioning control found an average positioning error of 1.01 $\pm$ 0.34 mm and a HIFU ablation accuracy 1.32$\pm$ 0.58 mm[45]. Another study investigated a hybrid control approach in HIFU therapy and found a robotic endpoint accuracy of 0.5 mm[44]. The accuracy and repeatability of using the custom software to control the six-DOF UR3 robot was found to be smaller than aforementioned results. Based on the results in this study, the proposed robotic positioning and monitoring approach is expected to significantly improve atherosclerotic plaque targeting during US-guided HIFU interventions.

Chapter 4 *In vivo* robot control of the transducer using the custom software

4.1 Introduction

To evolve high intensity focused ultrasound (HIFU) to a standard treatment modality for atherosclerosis, precise localization and transducer positioning will need to be investigated *in vivo.* Feasibility of using the UR3 robot and custom software to control the DMUA-transducer is investigated by targeting the dorsal wall of the femoral artery in porcine models during ultrasound (US)-guided HIFU therapy.

4.2 Materials and methods

In nine healthy porcine models (~50 kg), HIFU therapy was applied using the UR3 robot and the custom software. Animals were terminated on the same day (n = 3), after 3 days (n = 3) or after 14 days (n = 3) to analyze the target tissue after therapy. Ethical approval was granted by the Animal Welfare Body Utrecht.

Using conventional US, the femoral artery in the inguinal region was identified on one side and subsequently marked on the skin. A 3D mouse with a six degrees of freedom (DOF) sensor was used to control the UR3 robot for initial positioning of the DMUA-transducer onto the pig's skin. Subsequently, HIFU imaging, and transducer motion in the proximal and distal direction of the target artery were performed to identify the trajectory located inside the transducer's therapeutic field (ThxOF). Using the HIFU software, image quality was optimized and the required skin region, target region and the HIFU focus were set. Six to eight HIFU shots were delivered to the dorsal wall of the femoral artery, in 25 to 40 transverse planes spaced 1 mm apart in direction of the target artery. The number of shots in each plane varied depending on artery diameter.

The custom software was used to move and rotate the transducer with respect to the desired therapy locations. The axial and lateral HIFU coordinates, and corresponding 3D robot positions were saved to visualize all 3D ablation positions in real-time. The linear 3D distances between subsequent ablation position were displayed to allow for precise spacing and ensure partially overlapping lesions, thereby creating a confluent ablation zone.

4.3 Results

The workflow of HIFU therapy for atherosclerotic plaque targeting using the transducer, robot and accessories was optimized during the experiments (**Table 4.1**). Diagnostic US was performed to identify the target area prior to HIFU treatment (**Figure 4.1**).

Using the custom software, we were able to control DMUA-transducer motion with the UR3 robot (**Figure 4.2**). The transducer could be moved and rotated in all three orthogonal direction, with respect to either the skin or the HIFU focus. The custom software improved transducer positioning and monitoring during treatment, especially real-time distance feedback and visualization of the 3D ablation positions (**Figure 4.3**). The histology results are currently being analyzed, and will be published in the future.

The saved data was used to visualize the ablation positions of each experiment with respect to the transducer's ThxOF (**Figure 4.4**). In other words, the saved ablation positions for all treatment planes were plotted per experiment along with the transducer's ThxOF. For each graph, corresponding to one animal experiment, the percentages of HIFU ablations delivered outside the ThxOF are also calculated and visualized (**Figure 4.4**).

To identify potential improvements in the HIFU workflow, the saved times and data in the log file were analyzed. The data used for monitoring during HIFU therapy is summarized for each experiment, such as the number of shots, the number of planes, the mean distance between ablation positions, and duration of HIFU therapy (**Table 4.2**). Therapy duration and the time between subsequent shots and planes were calculated using the time saved with each of the saved robot poses. The mean number of shots, the number of planes and number of shots per plane for all HIFU experiments were 211, 33 and 6.4, respectively. The mean distance between subsequent ablations was 1.13 mm, which is close to the targeted 1 mm. Mean time to position the HIFU transducer was 16 minutes and 21 seconds, and varied from 2 minutes and 13 seconds, to 34 minutes and 7 seconds. Mean HIFU therapy duration was 2 hours, 2 minutes and 2 seconds, varying from 48 minutes and 50 seconds to 3 hours, 39 minutes and 3 seconds. The mean time per shot was 37 seconds, varying from 4 seconds to 4 minutes and 35 seconds for all experiments.

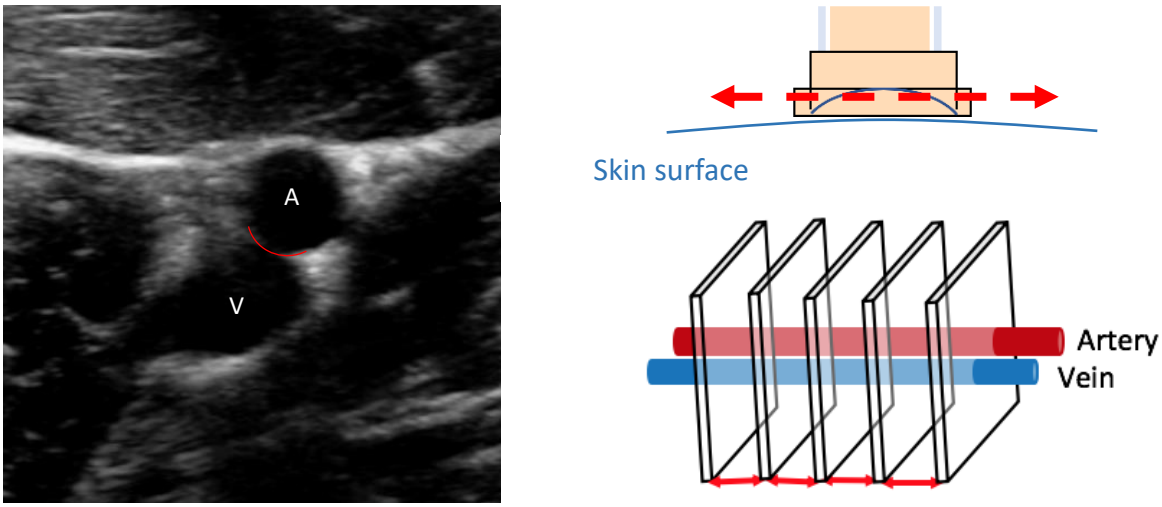

Figure 4.1 Target identification prior to HIFU therapy. **Left.** The femoral artery (A), vein (V) and the targeted dorsal arterial wall (red line) on diagnostic ultrasound. **Right.** Proximal and distal target verification during initial DMUA-transducer positioning (red dashed arrows).

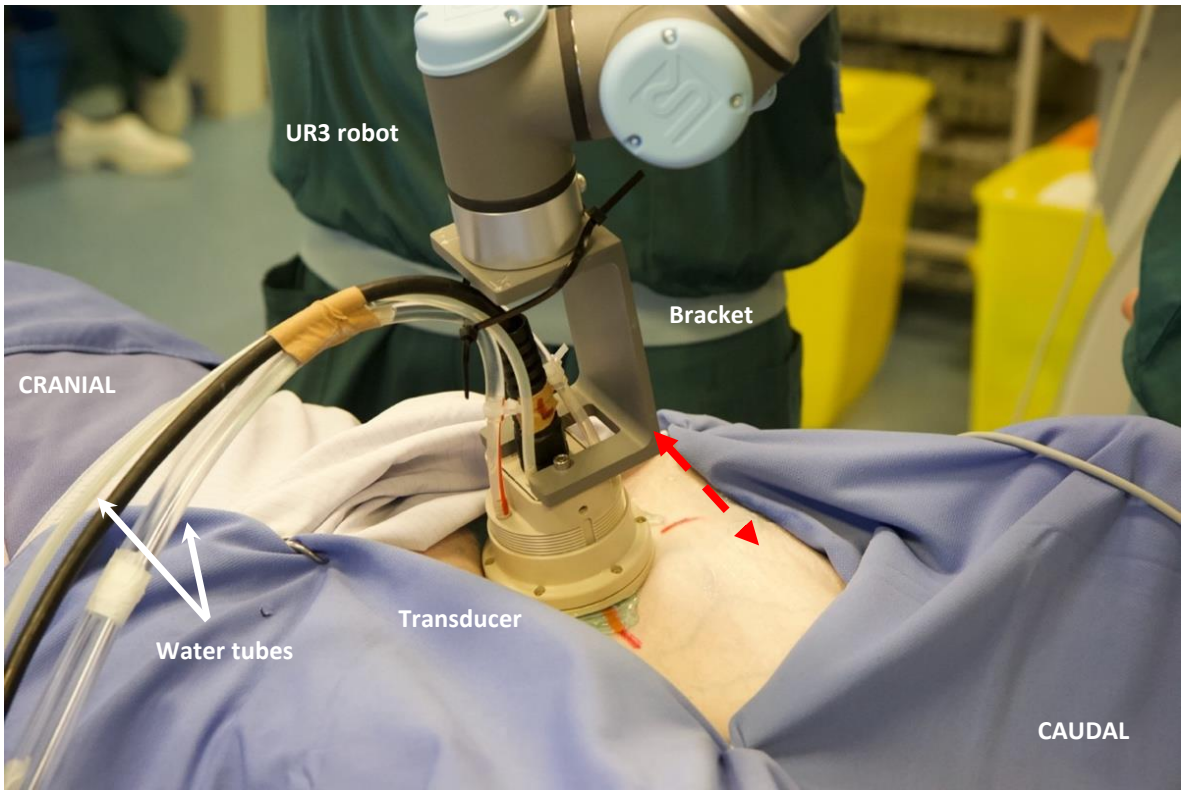

Figure 4.2 DMUA-transducer positioned onto the pig's skin during one animal experiment using the UR3 robot and bracket. The water tubes facilitate circulation of degassed water through the water bolus for US coupling to the region of interest (ROI). The ROI was marked on the skin (red lines under transducer). Proximal and distal target verification using the DMUA-transducer is illustrated (dashed red arrow).

Table 4.1 HIFU workflow during the preclinical animal experiments, categorized under the HIFU system, the UR3 robot and for other activities.

	HIFU system	UR3 robot	Other
PREPARATION	1. Start HIFU system and software	1. Start robot, computer and robot software	1. Fill bolus cover with degassed water
	2. Run FPGA tests	2. Connect robot software to robot	2. Attach water tubes to degassing system
	3. Attach transducer cable and thermocouples		3. Screw bolus cover onto the transducer
			4. Attach transducer and bracket to UR3 robot
			5. Shave inguinal region of porcine model
PRETREATMENT	4. Verify 35 – 40 image planes:		1. Perform diagnostic US
	a. Image target artery with HIFU	b. Move transducer in direction of artery	2. Mark target on skin
	5. Select skin region and target area		3. Position transducer in freedrive
HIFU THERAPY	1. Perform HIFU imaging		
	2. Select HIFU focus		
	3. Transfer HIFU focus coordinates	1. Save lateral and axial focus coordinates	
	4. Deliver HIFU shot	2. Check distance to previous HIFU focus	
	5. Check lesion control profile	3. Move transducer 1 mm after each plane	

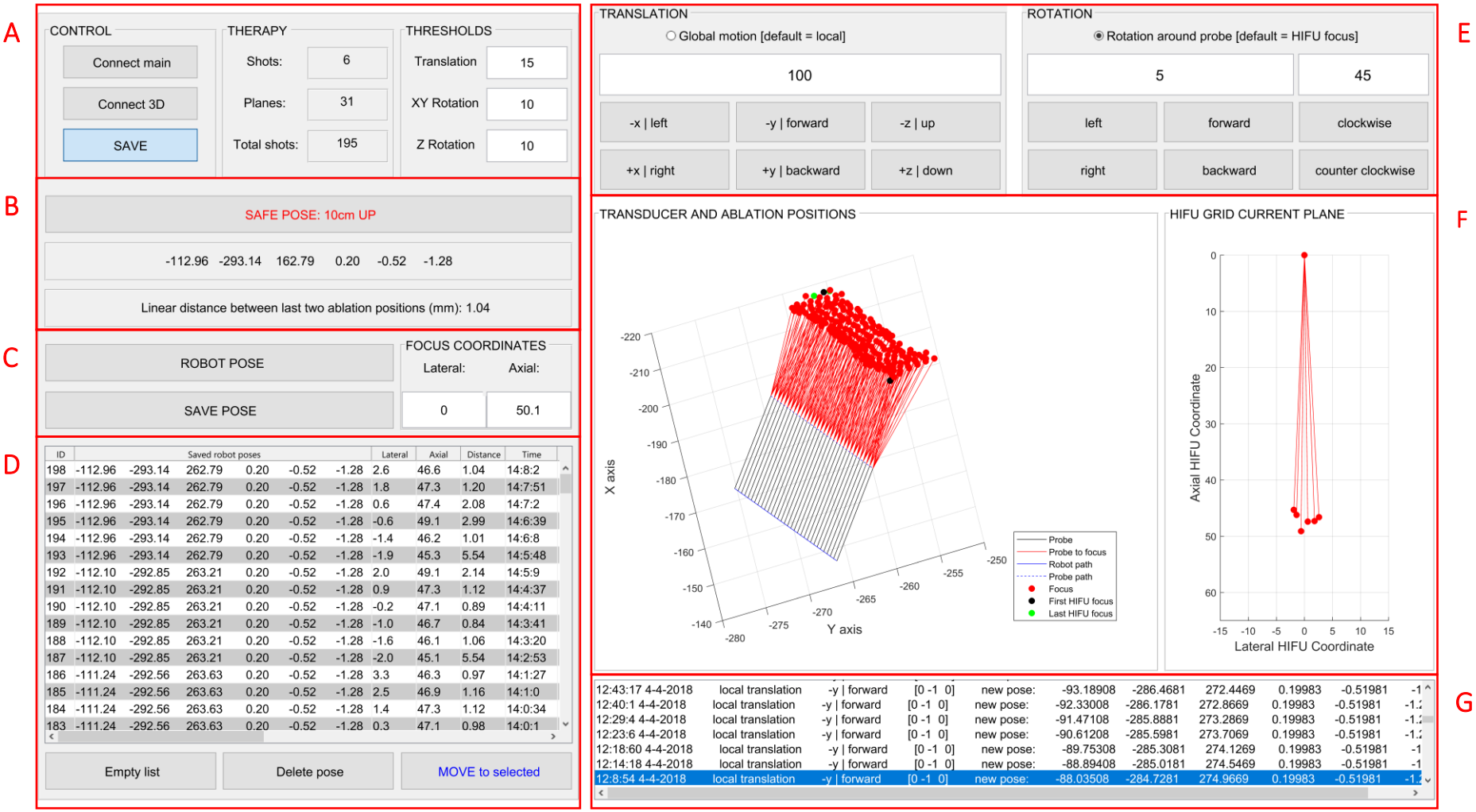

Figure 4.3 Graphical user interface (GUI) with saved robot poses and ablation positions of the third 14-days follow-up experiment. **Panel A:** Connect the robot to the GUI or a 3D mouse and save all data, control HIFU shots and treatment planes, and adjust robot motion thresholds. **Panel B:** Move the robot to a safe pose, display the current robot pose and the 3D distance to the previous ablation position. **Panel C:** Display and save the current robot pose with HIFU focus coordinates. **Panel D:** Saved robot poses with HIFU focus coordinates, the robot can be moved to each saved pose. **Panel E:** Execution of robot translations and rotations in x, y and z-direction. The UR3 robot can be translated in the orientation of the Tool (local motion) or the Base (global motion), and rotated around the transducer or the last saved HIFU focus. **Panel F:** Visualization of all 3D transducer and ablation positions, and the 2D ablation positions in the current treatment plane. **Panel G:** Events-file wherein all robot motion is displayed with time and magnitude.

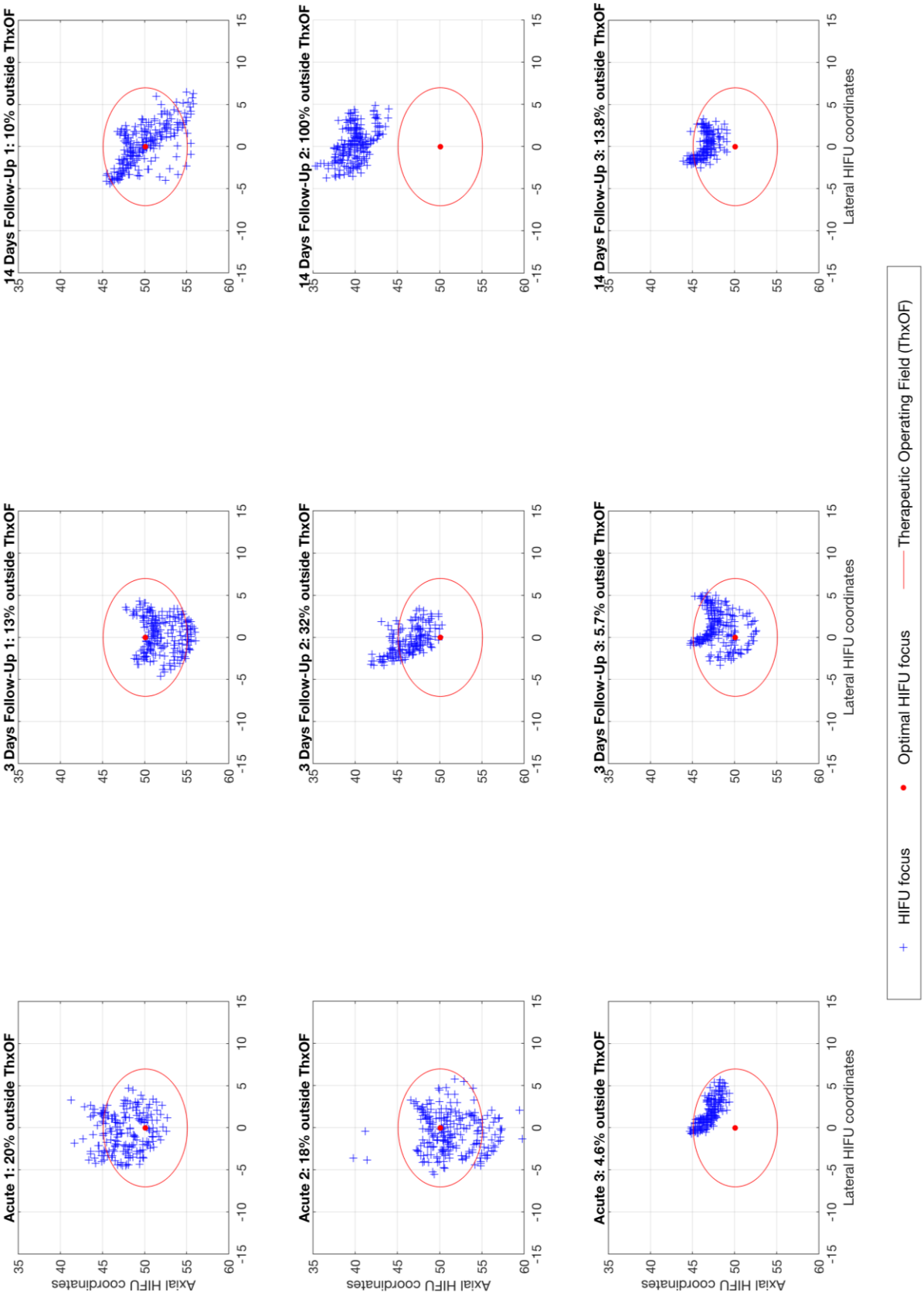

Figure 4.4 2D ablation positions with respect to the transducer's operating field (ThxOF). The axial and lateral HIFU coordinates are used to plot each HIFU focus per experiment in one figure, with the ThxOF.

Table 4.2 Summary of saved data in custom software for each animal experiment. FUP = Follow-up, S = shots, P = planes, D = distance, Pos. = positioning.
* Distances were not calculated and displayed during the experiment, and were calculated afterwards.
** Times were not saved with each saved robot pose, and the mean time per shot was calculated based on therapy duration and the total number of shots. The time between subsequent treatment planes were retrieved from the log file.

Robot pose	**TREATMENT**				**TIME**				
	S	**P**	**S/P**	**D** (mm)	**Pos.** (m:s)	**Therapy** (h:m:s)	**Per shot** (m:s)	**Per plane** (m:s)	**Pos. between planes** (m:s)
Acute 1	192	30	6.4 [4 – 8]	1.50 [0.73 – 3.79]*	12:13	03:39:33	01:09 [*not saved*]**	07:12 [00:58 – 65:04]**	
Acute 2	231	35	6.6 [6 – 13]	1.23 [0.51 – 2.61]*	36:53	02:45:03	00:43 [*not saved*]**	04:49 [01:00 – 27:26]**	
Acute 3	197	32	6.2 [5 – 8]	1.01 [0.50 – 1.86]	12:32	00:48:50	00:15 [*not saved*]**	01:39 [01:00 – 04:21]**	
3-days FUP 1	209	30	7.0 [6 – 8]	1.13 [0.51 – 2.06]	06:36	01:37:10	00:28 [*not saved*]**	03:11 [01:19 – 20:03]**	
3-days FUP 2	167	29	5.8 [4 – 7]	1.21 [0.74 – 3.19]	09:01	01:43:34	00:37 [00:05 – 04:35]	02:13 [01:02 – 06:45]	01:24 [00:24 – 04:13]
3-days FUP 3	230	35	6.6 [6 – 8]	1.15 [0.66 – 1.82]	19:55	02:32:27	00:40 [00:05 – 02:42]	03:25 [02:16 – 02:42]	00:58 [00:24 – 02:42]
14-days FUP 1	240	38	6.3 [6 – 7]	1.22 [0.35 – 2.61]	13:42	01:09:28	00:17 [*not saved*]**	01:45 [01:06 – 06:15]**	
14-days FUP 2	235	36	6.5 [5 – 7]	1.13 [0.48 – 2.02]	02:13	01:45:17	00:27 [00:04 – 03:45]	02:07 [01:16 – 04:06]	00:50 [00:22 – 03:45]
14-days FUP 3	195	32	6.1 [5 – 7]	1.08 [0.14 – 2.99]	34:07	02:28:22	00:46 [00:11 – 07:16]	03:12 [01:57 – 10:10]	01:07 [00:28 – 04:41]
Mean	211	33	6.4 [4 – 13]	1.13 [0.14 – 3.79]	16:21	02:03:18	00:36 [00:04 – 04:35]	03:17 [00:58 – 65:04]	01:05 [00:22 – 04:41]

4.4 Discussion

Therapy monitoring

As the distances between ablation position within the treatment planes ranges from 0.14 to 3.79 mm for all experiments, HIFU focus positioning can still be improved. To maintain the distances between all ablations around 1 mm, a warning can be implemented in the custom software which shows if the distance between the current and previous HIFU focus is smaller than 0.5 mm or larger than 1.5 mm. Doing so allows for replacement of the focus prior to HIFU energy delivery, and may thereby increase HIFU efficacy.

Through experience with the HIFU software and assessment of the lesion control profile, we have learned that the time between subsequent HIFU shots should at least be 30 seconds. This was achieved in 5 out of the 9 animal experiments. To ensure sufficient time between shots in the future, the custom software can be improved by adding an additional warning, or by blocking the possibility to enter HIFU coordinates, if the time between saved robot poses is less than 30 seconds.

The presented durations of initial transducer positioning were calculated using the times between starting the robot software and saving the first ablation position. It follows that larger intervals were observed if HIFU therapy was not immediately started after starting the robot. Total duration of HIFU therapy was calculated using the times the robot software was started and therapy was finished. Any delay during the experiments, for example due additional testing with the HIFU software or a break, was not accounted for. As the DMUA-transducer is controlled through a separate system, there was a discrepancy between the times saved in the custom software, and the moment the HIFU shots were delivered. As the workflow did not vary significantly between the HIFU shots and the separate experiments, the relative time differences between saving a robot pose and the delivery of a HIFU shot are not expected to vary greatly. Integration of the robot control software and HIFU system offer a solution for these limitations in the future, and may thereby improve efficacy during HIFU therapy.

In the second 3-days follow-up and second 14-days follow-up experiments, 32% and 100% of the HIFU shots were delivered outside the transducer's ThxOF, respectively. As explained in **Chapter 2**, targeting outside the ThxOF may lead to less unequivocal lesions due to a significant reduction in focusing gain (**Figure 2.2**). It is hypothesized that HIFU lesion formation was less efficient and less homogenous in these experiments, as opposed to HIFU energy delivery inside the ThxOF for all ablation positions. For the other experiments, targeting outside the ThxOF was 20% or less. HIFU ablations were performed outside the ThxOF as the HIFU settings needed optimization and the operators were not yet fully acquainted with the system, prior to this first set of animal experiments. In the analysis of the target tissue upon excision, it was difficult to differentiate between the induced HIFU lesions in each experiment with respect to the presented data. Histological analysis of the target tissues is currently being performed and will be analyzed in the future to link the clinical outcomes to the robot data.

As the software was under development during the experiments, the times were not yet saved with each ablation positions for the first three acute, the first 3-days follow-up and the first 14-days follow-up animal experiments. In these cases, the times between subsequent treatment planes were retrieved from the log file. For the other experiments, the time between saving the first and last robot pose were retrieved for each treatment plane. The intervals between the last robot pose of one treatment plane and the first robot pose of the next were used to calculate the duration of transducer positioning between subsequent planes. Mean positioning time between two subsequent planes was 1 minute and 5 seconds, varying from 22 seconds to 4 minutes and 41 seconds. The transducer was rotated and moved to position the target artery in the center of the HIFU image plane, and therapy was continued (**Figure 2.1**).

3D mouse control

Using the 3D mouse, each of the six robot axes can be controlled, which can improve initial positioning of the transducer with respect to the target artery. However, identifying the target artery by moving the transducer proximally and distally to image all treatment planes was rather difficult. As the 3D mouse is highly sensitive, steady and precise motion was required for each axis. As the UR3 robot is mounted upside down onto the steel frame, the 3D mouse was calibrated accordingly. However, as the robot configuration varied for each procedure, the axes of the 3D mouse were not always in alignment with the robot's motion axes, resulting in less intuitive motion control and decreased positioning speed. To overcome this limitation, the 3D mouse should be calibrated prior to each HIFU procedure, according to the robot configuration and location of the UR3 robot operator with respect to the robot. Additionally, training and experience of the UR3 robot operator is required to efficiently control the UR3 using the 3D mouse.

3D mouse positioning did not function properly during all experiments, as the same connection was used for control using the GUI. The GUI was connected to the UR3 robot throughout the HIFU procedures, and a separate software script was required to connect the UR3 robot to the 3D mouse. Additionally, the computer did not recognize the 3D mouse in all cases and a computer restart or driver update was required update was required, severely interrupting the HIFU workflow. In the future, seamless integration of the 3D mouse and the GUI is required, which can be realized by further improvement of the current software.

Water bolus and cover

The bolus cover is bulky, and momentum was required to screw the bolus cover onto the transducer. During multiple experiments, water leakage was observed at the level of the transducer. Increased water leakage was observed with increased transducer pressure exerted onto the pig's skin. To ensure effective imaging and HIFU energy delivery, refilling of the bolus or moving the transducer closer to the target artery was required. To maintain stable pressure, an additional water pump and pressure meter were used to monitor and change the water volume inside the bolus. Water pressure was restored after leakage by manually switching the pump on and off during a procedure. Although water pressure inside the bolus cover was more stable using the additional water pump, we did not manage to continuously monitor the water pressure and it was experienced as rather

laborious. We hypothesize that the isolating rubber ring between the bolus cover and the transducer may be wearing off, which was replaced after the final HIFU experiment and will be tested in future experiments. Alternatively, the bolus cover may need to be redesigned to lower the friction between the cover and the transducer, and by preventing water leakage. This is expected to improve the current workflow during a HIFU procedure, as less time is required to screw the bolus cover onto the transducer, and continuous monitoring and refilling of the bolus may be eliminated.

3D visualization robot, transducer and ablation positions during HIFU therapy

3D lines representing the distal end of the robot, the distal end of the transducer, and the HIFU focus are currently visualized for each separate ablation position. The visualized 2D and 3D ablation positions were sufficient for monitoring during the experimental procedures. However, due to the many possible robot configurations and varying transducer orientations, it was sometimes difficult to translate the visualizations to the actual setup during a procedure. It may prove beneficial in the future to add a more detailed visualization of the transducer orientation and robot configuration, e.g. a cylindrical volume with markings to denote its orientation with the current visualized line at its center. Different colors can be used for the transducer and the robot, respectively. Additionally, the transducer, robot and HIFU foci were visualized relative to each other based on the saved robot poses. We currently do not have a reference to the actual pig visualized.

The custom software visualizes the ablation positions perpendicular to the transducer's imaging plane. However, if the transducer is not positioned completely perpendicular to the target artery, the visualizations were not aligned in direction of the target artery. In five animal experiments, left-right shifts were observed between subsequent treatment planes as a result of this limitation (**Figure 4.5**). If the target artery moved outside the transducer's therapeutic operating field due tortuosity, the robot was used to position the transducer with the target artery in the center of the HIFU imaging plane again. During the HIFU procedures, perpendicularity was assessed after saving ablation positions for multiple treatment planes. Subsequently, this was corrected for by rotating the transducer in the z-direction, until the direction of the target artery was completely perpendicular to the HIFU image plane. To overcome this limitation in the future, multiple robot poses can be saved during initial positioning of the transducer using fictional HIFU coordinates. Although, this requires more time prior to HIFU therapy, it is expected to improve the visualizations with respect to the HIFU imaging plane and target artery during the procedure.

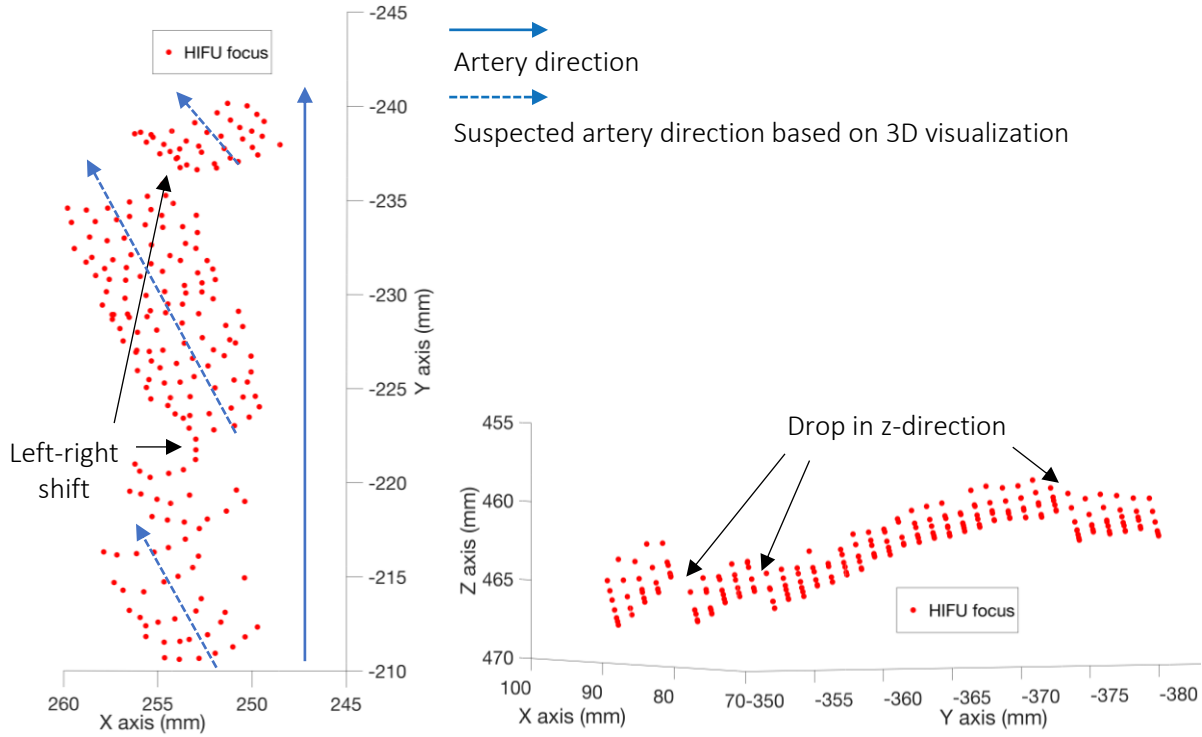

Figure 4.5 3D ablation positions with direction of treated artery. Left. Left-right shift between subsequent transverse treatment planes during the first 3-day animal experiment (top view). Right. Drops in z-direction between subsequent transverse treatment planes during the second 14-day animal experiment (side view).

Aforementioned variation in the bolus volume during the experiments resulted in varying heights of the visualized ablation positions using the custom software (**Figure 4.5**). Sudden drops in the z-direction between subsequent treatment planes were observed as the transducer needed to be moved closer towards the target artery as a result of a gradually decreased water bolus. The resulting visualizations potentially suggest that the corresponding HIFU ablation positions were not adjacent, while HIFU imaging confirmed adjacent treatment planes and ablations. Improving the software or preventing water leakage can overcome this limitation.

Integrating the HIFU software and the robot control software

The HIFU software and robot control software are installed on separate systems, and the axial and lateral HIFU coordinates needed to be transferred verbally for each ablation position. A mean of 422 coordinates were verbally transferred during the HIFU procedures (**Table 4.2**). It was difficult to verbally transfer the coordinates due to the relatively high levels of noise of the HIFU system and the UR3 robot. Combined with manual entering in the custom software, saving the HIFU coordinates was experienced to significantly interrupt the HIFU workflow. Ideally, the actual HIFU coordinates are transferred automatically from the HIFU system to the robot control software when a HIFU shot is delivered. Additionally, the distance between ablation positions is displayed in the custom software and monitoring is performed by the robot operator. HIFU efficacy and monitoring is expected to improve by displaying the distance between the previous HIFU focus directly in the HIFU software when a new HIFU focus is selected. Doing so allows for direct changes of the HIFU focus prior to delivery of a HIFU shot, thereby ensuring adjacent lesion formation.

4.5 Conclusion

In nine animal experiments, the feasibility of robotic DMUA-transducer control during noninvasive HIFU surgery for atherosclerotic plaque targeting was demonstrated *in vivo*. This was the first set of *in vivo* experiments to optimize the HIFU settings, robot control and workflow within our research group. There is room for optimization of the robot software, which was still under development during the experiments, as well is HIFU energy delivery inside the transducers ThxOF. Additional warnings and safety features can be implemented to improve monitoring of HIFU energy delivery.

Using a six-DOF robot and custom robot control software allowed for the real-time visualization and feedback of the therapy locations. As opposed to manually positioning the transducer or using robotic manipulators with fewer degrees of freedom, the HIFU workflow was significantly increased and potentially increased therapeutic success. Integration of the separate HIFU system and robot control system may further increase the workflow by enabling for direct feedback of the HIFU coordinates and distance between ablation positions. We hope that this research is a first step towards the clinical implementation of our robotic HIFU surgery approach.

Chapter 5 Targeting the lower-extremity arteries in patients suffering from peripheral artery disease

5.1 Introduction

Using the experimental setup, high intensity focused ultrasound (HIFU) shots can be delivered within the dual-mode ultrasound transducer's axial and lateral range. Optimal HIFU delivery occurs inside the transducer's therapeutic operating field (ThxOF), an elliptical region around the transducer's geometric focus (50.1 mm), laterally and axially extending ±7 mm and ±5 mm, respectively. The transducer range is hardware-limited and cannot be changed using the software. As we aim to treat patients with this setup in the future, it is important to determine which patients suffering from peripheral artery disease (PAD), and which femoral artery trajectories, are most suitable for HIFU therapy with respect to the transducer's depth range. Moreover, not all patients may be suitable for HIFU therapy due to interpatient variation in arterial tortuosity. The aim of this study is to investigate the depth of the common femoral artery (CFA), superficial femoral artery (SFA) and popliteal artery (PA). Additionally, this may help to determine the optimal depth range of HIFU transducers to treat the majority of patients suffering from PAD, and indicate the need for the development of transducers with varying depth ranges in the future.

5.2 Methods

5.2.1 Patient population

We retrospectively have analyzed magnetic resonance angiographic (MRA) images of 25 patients treated with percutaneous transluminal angioplasty and/or stenting in the aortoiliac- and femoropopliteal regions at the University Medical Center Utrecht. MRAs were acquired between 04-11-2014 and 06-06-2018. Patients with chronic total occlusions in the aortoiliac- or femoropopliteal arteries were excluded, as visualizations were unreliable due to a lack of contrast medium in these regions. Scans in which no skin was visible in the transversal plane were also excluded, as no reliable measurements could be performed.

5.2.2 MRA data acquisition

MRA data was acquired with 1 mm slice thickness using an Enhanced T1 High Resolution Isotropic Volume Excitation sequence (e-THRIVE, Philips, Amsterdam, The Netherlands) on a 1.5 Tesla MRI system (Philips Ingenia 1,5T, Philips, Amsterdam, The Netherlands) with Gadolinium-based contrast media.

5.2.3 Study design

Depth of the CFA, the SFA, and the PA were measured in the transverse planes of the MRAs using 3mensio Vascular (Pie Medical Imaging, Maastricht, The Netherlands). Starting 10 cm below the iliac bifurcation and stopping at the PA at knee level, measurements were performed every 0.8 to 3.2 cm in the cranial-caudal (CC) direction. Based on visual inspection of arterial tortuosity, measurements were performed more or less frequent in the CC direction. In each transverse slice, the artery diameter and the shortest distance between, and perpendicular to, the skin and the dorsal arterial wall (the arterial wall furthest from the skin) was measured on the left and the right side.

The radiology reports corresponding to each MRA were used to summarize lesion presence in all patients, for the Common Iliac Artery (CIA), External Iliac Artery (EIA), Internal Iliac Artery (IIA), CFA, SFA, Profunda Femoral Artery (PFA), PA, Anterior Tibial Artery (ATA), Posterior Tibial Artery (PTA) and Fibular Artery (FA). Lesion presence was used to determine which arteries are most effected by PAD in this study, and which arteries may need to be targeted with HIFU therapy in the future.

5.2.4 Statistical analysis and data visualization

Statistical data analysis and visualization was performed using MATLAB (Version R2017a, MathWorks, Inc., Natick, MA, USA). Measurements of the individual patients were linearly interpolated to 1000 data points, and the mean, the standard deviation, and the 95% confidence interval (CI) were calculated. The 95% CI of the artery depths were visualized, along with the transducer's depth range, i.e. 45.1 to 55.1 mm, and an increase of the therapeutic operating field of ±3 mm. To visualize the transducer range starting from the patient's skin, the minimum axial distance required by the bolus cover (15 mm) was subtracted from the transducer's axial ThxOF.

The percentages of the artery trajectories inside the ThxOF, inside the additional region, and outside the transducer's therapeutic range were calculated per patient and subsequently averaged to calculate the 95% CI for all patients. Percentages were calculated for the frontal and dorsal wall separately, as well as for targeting both arterial walls in each patient.

5.3 Results

The distances from skin to frontal and dorsal arterial walls were measured (**Figure 5.1** and **Figure 5.2**). Seventeen male and eight female were included in this study (**Table 5.1**).

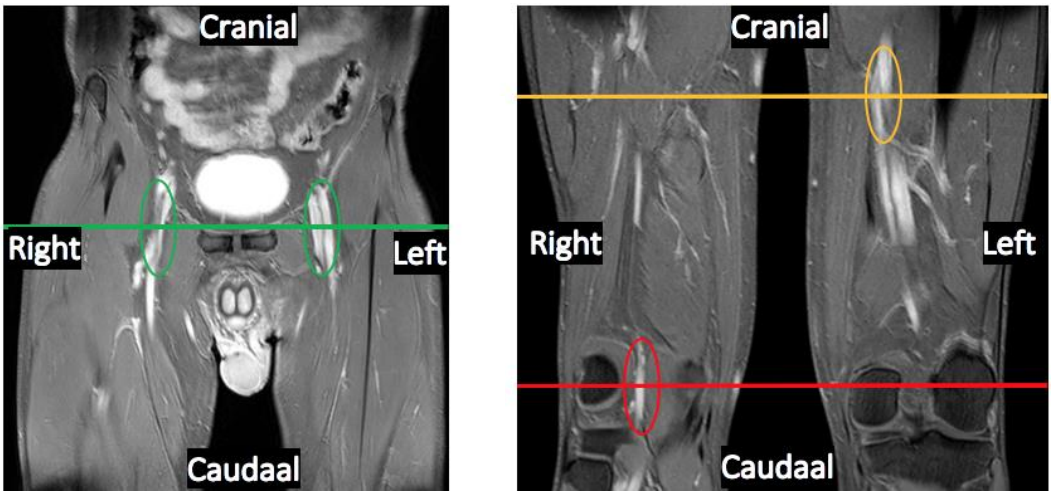

Figure 5.1 Coronal magnetic resonance angiographic (MRA) reconstructions with axial levels of measurements performed in a patient. **Left.** Abdominal MRA with level of left and the right common femoral artery measurements (green line and circles). **Right.** Upper leg MRA with levels of measuring the left superficial femoral artery (orange line and circle) and the right popliteal artery (red line and circle).

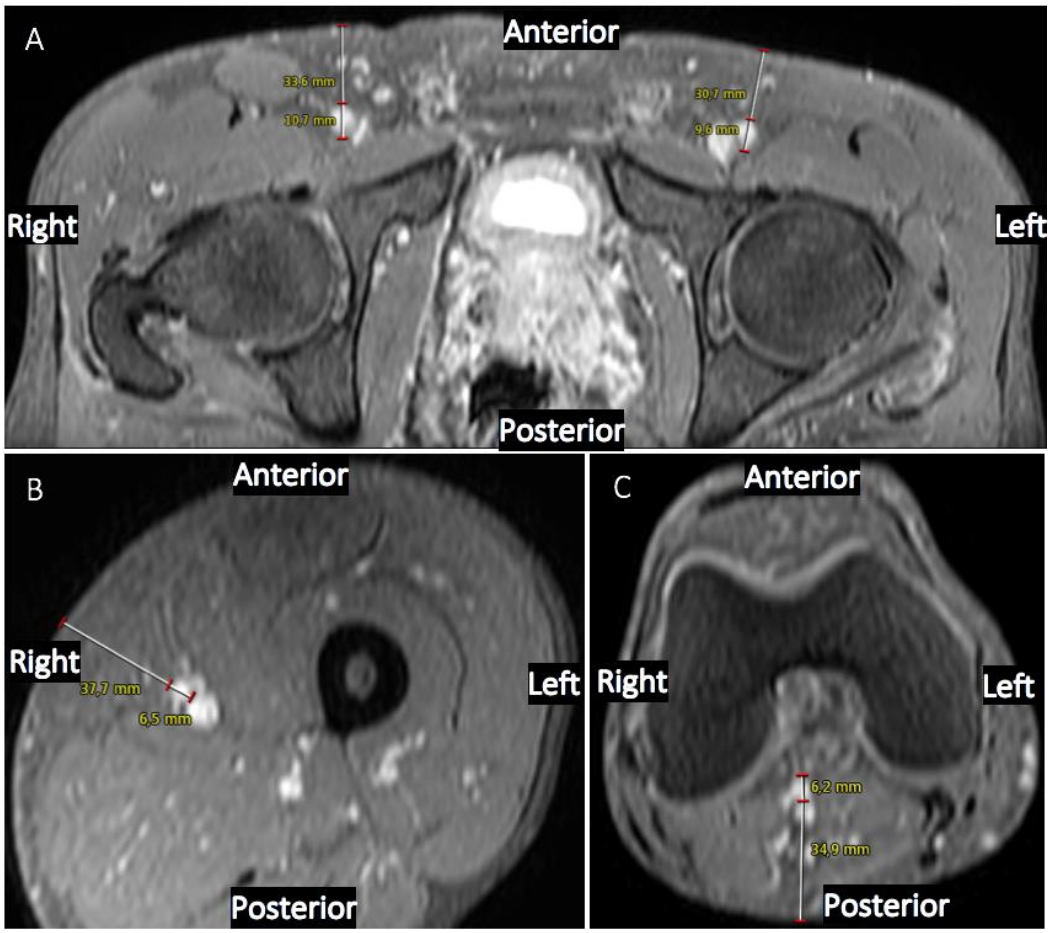

Figure 5.2 Transverse magnetic resonance angiographic reconstructions of a patient with artery diameters (smallest distance) and the distances from the skin to the dorsal arterial wall (greatest distance). **A:** Depth of the common femoral artery. **B:** Depth of the superficial femoral artery. **C:** Depth of the popliteal artery.

Table 5.1 Characteristics of 25 patients included.

Patient characteristics	Median	Range
Age (years)	68	40 - 81
Length (cm)	176	160 - 200
Weight (kg)	83	54 - 135
Body Mass Index (kg/m^2)	25.6	19.4 - 37.4
Gender	17 male	8 female

The mean distance in CC direction over which measurements were performed was 60.4 cm (range 36.0 – 94.8). The mean artery depths and corresponding 95% CI between the first measurement slice and the PA at knee level are visualized for the left and the right side, with respect to the transducer's axial ThxOF (**Figure 5.3**).

The mean percentages and 95% CI of the artery trajectories inside the ThxOF, inside the additional region, and outside the transducer's therapeutic range were calculated (**Table 5.2**). In all patients, the arteries enter the transducer's depth range between the iliac bifurcation and the femoral bifurcation.

The reported lesions per artery were identified for each patient (**Appendix 5.A**), and summarized for all patients (**Table 5.3**). On the left side, a stent or bypass was most common in the CIA (n = 4), followed by the EIA (n = 2) and SFA (n = 2). A significant stenosis, i.e. ≥50% lumen decrease, was most common in the SFA (n = 13), followed by the CIA (n = 5) and EIA (n = 5). On the right side, a stent or bypass was most common in the CIA as well (n = 8), followed by the EIA (n = 4). A significant stenosis was most common in the ATA (n = 6), followed by the SFA (n = 5).

Table 5.2 Mean percentages of the artery trajectories inside the transducer's axial therapeutic operating field (ThxOF), inside the extended (EXT) ThxOF, and outside the therapeutic range, with the 95% CI between brackets.

Side:	Left		Right	
Wall section:	Frontal	Dorsal	Frontal	Dorsal
ThxOF (%)	37.3 [27.3 – 47.4]	31.0 [20.4 – 41.6]	36.6 [28.4 – 44.9]	31.8 [20.4 – 43.2]
EXT ThxOF (%)	53.2 [42.5 – 64.0]	45.3 [31.8 – 58.8]	54.1 [44.7 – 63.6]	47.6 [33.8 – 61.4]
Outside ThxOF (%)	46.8 [36.0 – 27.5]	54.7 [41.2 – 68.2]	45.9 [36.4 – 55.3]	52.4 [38.6 – 66.2]

Table 5.3 Number of lesions reported per artery for all patients. CIA = Common Iliac Artery, EIA = External Iliac Artery, IIA = Internal Iliac Artery, CFA = Common Femoral Artery, SFA = Superficial Femoral Artery, PFA = Profunda Femoral Artery, PA = Popliteal Artery, ATA = Anterior Tibial Artery, PTA = Posterior Tibial Artery, FA = Fibular Artery.

	CIA	EIA	IIA	CFA	SFA	PFA	PA	ATA	PTA	FA
	LEFT									
Significant stenosis (>50%)	5	5	2	1	13	2	3	2	3	2
Stent / bypass	4	2	0	0	2	0	0	0	0	0
	RIGHT									
Significant stenosis (>50%)	1	0	2	3	5	0	0	6	4	2
Stent / bypass	8	4	0	0	0	0	0	0	0	0

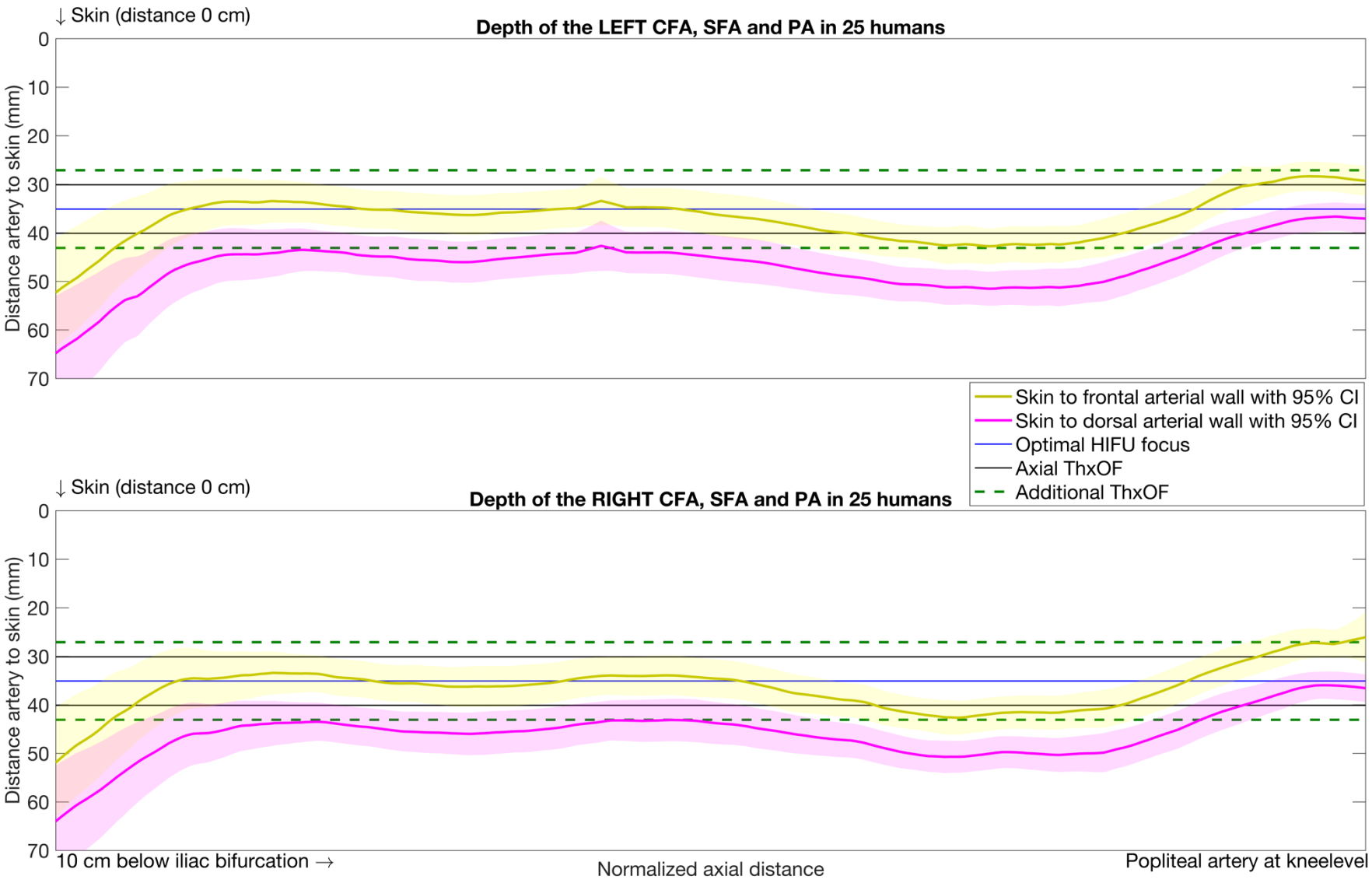

Figure 5.3 Mean and 95% CI of distance from skin to frontal and dorsal arterial wall in 25 patients, for the left and the right side. CFA = Common Femoral Artery, SFA = Superficial Femoral Artery, PA = Popliteal Artery, CI = Confidence Interfal, HIFU = High Intensity Focused Ultrasound, ThxOF = Therapeutic Operating Field.

5.4 Discussion

In the present study we find that 53.2% and 54.1% of the frontal artery trajectories are located inside the additional ThxOF on the left and right side, respectively. For the left and right dorsal artery trajectory, 45.3% and 47.6% is located inside the additional ThxOF, respectively. 54.7% and 52.4% of the dorsal arterial wall is located outside the additional ThxOF for the left and the right side, respectively. On the left and right side, 26.2% and 27.0% of the artery trajectory is located inside the additional ThxOF for both the frontal and dorsal arterial walls, respectively.

Patient inclusion

The number of PAD patients suitable for HIFU therapy in the future may be limited as a result of the transducer's axial ThxOF with respect to the artery depths. This limitation is especially evident in patients with higher BMI, wherein arteries are located further from the skin. Additionally, suitability for HIFU therapy depends on the location of the target lesion. On the left side, the most commonly treated or stenotic arteries were the CIA, EIA, SFA and CFA. On the right side, the CIA and EIA were most commonly treated, while significant stenoses were most commonly reported for the ATA, SFA and CFA. In all patients, the arteries enter the transducer's depth range between the iliac bifurcation and the femoral bifurcation. Therefore, lesions located in the CIA cannot be treated with the current transducer's depth range as used in this study. Due to great interpatient variation in arterial tortuosity and lesion presence, it is important to measure the distance to targeted plaques for each individual patient. Both the CFA and SFA are affected in these studies and may be suitable for HIFU targeting. Additionally, it may be useful to investigate targeting of the arteries in the lower leg as well in the future, especially as these arteries are located less far from the skin with respect to the upper leg and abdomen.

Axial distance required by the bolus cover

The axial distance required by the bolus cover in combination with the concave transducer design ranges from 15 to 25 mm, depending on how far the bolus cover is screwed onto the transducer (**Figure 5.4**). The geometric focus of the DMUA-transducer is assumed to be 50.1 mm, based on the average radius of curvature of manufactured transducers, i.e. 50.1 $\pm$0.05 mm (Measurement reports SN 11859 and 11859 1002, Imasonic Inc., Voray sur l'Ognon, France). To bring the transducer's optimal focus closer to the target arteries, the axial distance from skin to the target area may be decreased with some degree due to tissue compression by the transducer. Additionally, the distance required by the bolus cover may need to be decreased in the development of future bolus covers. In areas where the arteries are too close to the DMUA-transducer, i.e. at the level of the PA, the distance required by the bolus cover can be increased by adding water to the bolus, or by screwing the bolus cover less far onto the transducer.

Therapeutic operating field and HIFU intensity distribution

The 95% CI of the artery depths were visualized with respect to the adjusted axial ThxOF, and an additional region of ±3 mm. As HIFU intensity decreases rapidly outside its geometric focus, targeting outside the ThxOF may lead to less unequivocal lesions and should therefore only be performed occasionally (**Figure 5.5**).

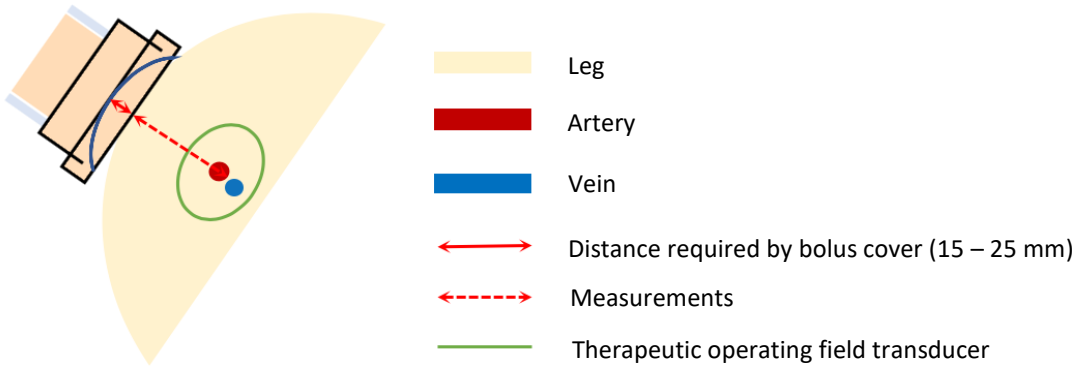

Figure 5.4 Distance required by bolus cover illustrated with respect to performed measurements and the transducer's therapeutic operating field.

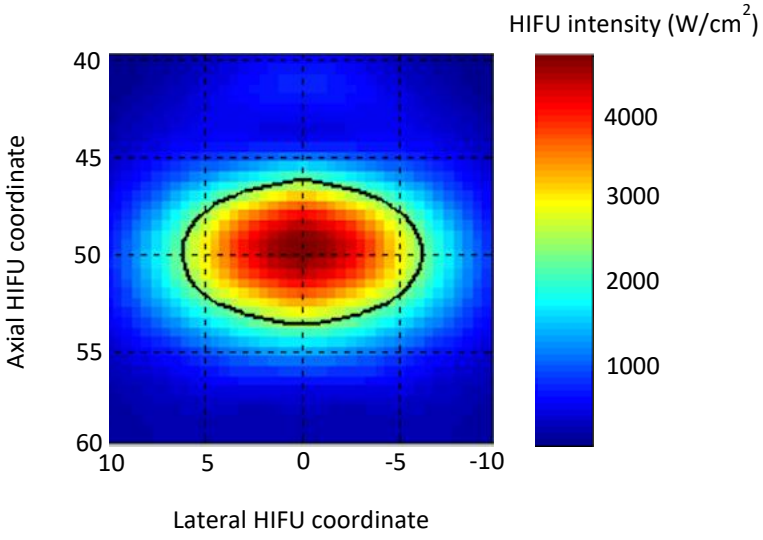

Figure 5.5 HIFU intensity distribution around the transducer's geometric focus (lateral value 0 mm, axial value 50.1 mm).

Limitations

No reliable measurements could be performed if the skin was not visible in the transversal MRA reconstructions, which was especially evident in the aortoiliac region in patients with higher BMI. These patients were therefore excluded. Consequently, the average BMI of the selected patients may be an underestimation of the average BMI of patients suffering from PAD. Additionally, the transversal field of view may need to be increased to fully image the abdomen of each patient in the acquisition of pre-operative MRAs.

Measurements were performed every 0.8 to 3.2 cm in the CC direction, with an increase in areas of great arterial tortuosity and vice versa. Due to a difference in patient lengths and measurement interval between patients, data interpolation was needed to create uniform datasets and allow for comparison, incorporating some level of uncertainty. Moreover, arterial tortuosity was subjectively assessed based on visual inspection.

5.5 Conclusion

For the left and right dorsal artery trajectory, 45.3% and 47.6% is located inside the additional ThxOF, respectively. The distance from the transducer to the target artery may vary due to the axial distance required by the bolus cover and due to tissue compression at the level of the transducer-skin interface. Large variation in arterial tortuosity between patients was found. Therefore, the distance to the targeted plaques needs to be measured for each individual patient before considering HIFU therapy. The iliac arteries were not inside the transducer's depth range and can therefore not be targeted using the current transducer. Lesions were also reported for the lower extremity arteries and it may be useful to investigate targeting these trajectories in the future.

The BMI of the patients included in this study may be an underestimation of the average BMI of patients suffering from PAD, which needs to be considered in selecting suitable patients for HIFU treatment in the future. Additionally, the transversal field of view may need to be increased to fully image the abdomen of each patient in the acquisition of pre-operative MRAs. These findings stress the need for careful patient selection and treatment planning, prior to HIFU therapy.

Appendix 5.A Lesions reported on MRA images in all included patients

	LEFT										RIGHT									
	CIA	EIA	IIA	CFA	SFA	PFA	PA	ATA	PTA	FA	CIA	EIA	IIA	CFA	SFA	PFA	PA	ATA	PTA	FA
Patient 1	4	3	0	1	3p	0	0	0	0	0	4	4	0	0	0	0	0	0	0	0
Patient 2	4	1	1	0	3p	0	0	0	0	0	4	1	1	0	1,2p	0	0	0	0	0
Patient 3	0	0	0	0	0	0	0	0	0	0	0	0	0	0	3p	0	0	3m	0	0
Patient 4	0	0	0	0	3	0	0	3	2	0	1	1	0	0	2p	0	?	0	0	3p
Patient 5	0	0	0	3	3m+	2p	2	0	3	0	4p	0	2p	0	1,2m	2p	0	0	3	0
Patient 6	3	0	2	0	1,3m	0	0	0	0	0	0	0	3	0	2p	0	0	3p	2+	2+
Patient 7	0	0	0	0	3p	0	3	0	0	0	0	0	0	3	3m	2p	0	0	0	0
Patient 8	0	0	0	0	0	0	0	0	0	0	0	0	0	0	0	0	0	0	0	0
Patient 9	4,3d	0	0	0	1p	0	0	0	0	1	4	0	0	0	1p	0	0	0	0	1
Patient 10	4	4	0	0	0	0	3	0	0	1	4	4	0	0	0	0	1	0	0	0
Patient 11	3	0	0	0	3p	0	0	0	0	0	0	0	0	0	3d	0	0	0	0	0
Patient 12	4	4	0	0	1	1	0	0	0	0	4	0	0	0	0	0	0	3+	0	0
Patient 13	0	0	0	2	0	0	0	0	0	0	0	2d	0	0	0	0	0	3	3d	3p
Patient 14	0	3p	0	0	3m	0	0	0	0	0	0	4	0	0	0	0	0	0	0	0
Patient 15	3	3	3	0	0	0	0	0	0	0	0	4	0	0	0	0	0	0	0	0
Patient 16	3m	0	0	0	0	0	0	0	0	0	2m	0	0	0	0	0	0	0	0	0
Patient 17	0	0	0	0	0	0	0	0	0	0	4	0	0	0	0	0	0	0	0	0
Patient 18	0	0	0	0	0	0	0	0	0	0	0	0	0	0	3m	0	0	0	0	0
Patient 19	0	0	3p	0	1,3m	3p	1	2+	2+	2+	0	0	3p	0	1p	1,2p	0	2	3d	2
Patient 20	0	0	0	1	1d	0	0	0	0	0	0	0	0	1	0	0	0	0	0	0
Patient 21	0	0	1	0	1+	0	0	2p	3p	2	0	0	0	0	1,2m	0	0	3p	0	0
Patient 22	4	0	0	0	4,3d+	0	0	0	0	0	0	0	0	0	2+	0	0	0	0	0
Patient 23	2	3	2p	0	3p	0	0	0	0	0	1	0	0	3	0	0	0	0	0	0
Patient 24	0	0	0	1	3p,4m	3p	3p	0	3	0	4	0	2p	0	0	0	0	0	0	0
Patient 25	3m	3m	0	0	3p	0	0	3	2	0	3d	0	0	3	1,3	0	0	3p	3p	0

Figure 5.6 Reported lesions on MRAs; 0 = no anomalies reported, 1 = mild atherosclerosis / mild wall irregularities / mild calcifications, 2 = stenosis <50%, 3 = stenosis ≥50%, 4 = stent / bypass present; p = proximal, m = mid, d = distal, + = multiple lesions. CIA = Common Iliac Artery, EIA = External Iliac Artery, IIA = Internal Iliac Artery, CFA = Common Femoral Artery, SFA = Superficial Femoral Artery, PFA = Profunda Femoral Artery, PA = Popliteal Artery, ATA = Anterior Tibial Artery, PTA = Posterior Tibial Artery, FA = Fibular Artery.

Chapter 6 General discussion

6.1 Results and limitations

The accuracy, safety and feasibility of robotic DMUA-transducer control was investigated during preliminary and *in vivo* experiments, using the HIFU system with a DMUA-transducer and a UR3 robot.

Experimental setup

Several improvements of the experimental setup are required to improve HIFU workflow during a procedure. During the first experiments, HIFU software improvements were identified, which are currently being implemented. During one animal experiment, we treated one side with the sub-therapeutic HIFU shots, e.g. only 20% of the HIFU amplitude was delivered, as opposed to the desired 80%. During this experiment, we started over at the other side with prescription HIFU shots. A change in software-design was proposed, and is currently being implemented to decrease the risk of delivering HIFU shots with suboptimal settings. Additionally, with our HIFU software we can select one ablation position and deliver one HIFU shot at a time. We know of another HIFU system which has the possibility to select multiple HIFU foci and deliver HIFU shots for the entire HIFU imaging plane at once. Combined with the integration of the robot control software, and automatically calculated distances between the ablation positions, this would really advance the HIFU workflow in the future.

The steel frame and the HIFU system were experienced to be bulky, and required a lot of space in the operating room. If HIFU can become a standard treatment modality for atherosclerosis in the future, the experimental setup needs to be more compact. The UR3 robot could be attached to a flexible arm mounted onto the ceiling, instead of a large steel frame. The HIFU system and robot control software can be integrated, and may eventually be combined in a control room, as opposed to two relatively large mobile systems in the OR. The bolus cover did not function optimally, as water leakage was observed and refilling of the bolus or repositioning of the transducer was required to maintain stable HIFU imaging. Water leakage need to be assessed in the future after replacement of the rubber ring between the bolus cover and the transducer. At last, the HIFU system and UR3 robot produced relatively high levels of noise during the procedures, mainly due to the cooling fans of the HIFU system, which may need to be addressed in the future.

Accuracy and repeatability of UR3 robot control

Accuracy and repeatability of the UR3 robot and the custom software was investigated. Robot translations and rotations were smaller than 0.1 mm and 0.1°, respectively, except for robot rotations around the HIFU focus. Error of rotation around a HIFU focus was likely higher due to positioning inaccuracies during the robot experiments, and may need to be tested in 3D in the future, as opposed to the performed 2D measurements.

Safety measures

The required safety measures of using the UR3 for transducer positioning were investigated and implemented using Polyscope and the custom software. Polyscope was used with its normal safety limits, e.g. the general maximum force, power, speed and momentum of the UR3 robot were 150 N, 300 W, 1500 mm/s and 25 kg m/s, respectively. As the UR3 robot configuration changes during a HIFU procedure, limiting the position of the individual joints was not desired. Based on preliminary testing, the linear speed limit of the TCP was limited to 0.2 mm/s in the dedicated Polyscope program, designed to execute robot motion from the custom robot software. To prevent robot collision with people and other equipment in its vicinity, it is advised to configure safety planes for the TCP position prior to each separate HIFU procedure, adjusted to the specific robot configuration and location in the operating room. During the experiments, the UR3 robot was positioned at the side we aimed to treat, perpendicular to the pig. The safety planes can be configured such that an emergency break occurs if the robot moves away from the target tissue, towards other equipment or towards the steel frame. A small working area perpendicular to the patient and slightly larger than the length of the aimed target artery should be allowed. Backward translations may cause the robot to collide with itself or the steel frame and should be limited accordingly. Forward translations are needed to treat the other side during a HIFU procedure, however, excessive forward translations may cause an emergency break at the UR3 robot's maximum reach, i.e. overstretching at 500 mm from its Base.

Artery depths in patients with respect to the ThxOF

To investigate which patients suffering from PAD, and which arterial trajectories are most suitable for HIFU therapy, artery depths in human patients were retrospectively analyzed. Due to great interpatient variation in artery depths, we were not able to identify specific arterial trajectories suitable for HIFU therapy in all patients. We concluded that for each individual patient, the distance to the targeted plaques need to be measured before considering HIFU therapy. Artery depths could not be measured reliably in patients with higher BMI, and it follows that most of the target arteries in these patients are not located inside the transducer's therapeutic depth range. To allow for artery depth evaluation of these patients, the transversal FOV can be adjusted during MRA acquisition. Measurements in patients with higher BMI can provide data on suitability of these patients for HIFU therapy and the required depth range in the potential development of future HIFU transducers.

Aiming to treat the majority of patients, DMUA-transducers with a therapeutic (depth) range customized for the general population of patients suffering from PAD could be developed. We concluded that the arteries were not inside the transducer's depth range before the first measurement slice, i.e. 10 cm below the iliac bifurcation. However, we only quantified artery depths from iliac bifurcation to the popliteal artery at knee level, while many patients (also) suffer from lesions in the popliteal artery below knee level. Lesion occurrence in the included patients was assessed based on the radiology reports corresponding to the MRA images. On the left side, the most commonly treated or stenotic arteries were the common iliac artery, external iliac artery, superficial femoral artery and common femoral artery. On the right side, the common iliac artery, external iliac artery, anterior tibial artery and superficial femoral artery were most commonly treated or stenotic. Based on this study,

the axial therapeutic range need to be increased to include (parts of) the common iliac artery and external iliac artery in the future. Alternatively, the distance between the concave-shaped transducer and the bolus cover may need to be decreased to bring the transducer closer to the target arteries.

Additionally, it is important to extend the current research with artery depths below knee level. As the PA at knee level was either too close to, or inside the transducer's ThxOF and the lower leg is generally smaller in diameter than the upper leg, it is hypothesized that the lower leg may be more suitable for HIFU therapy using the current DMUA-transducer as opposed to treatment of the upper leg and abdomen.

In vivo use of the robotic DMUA-transducer control

As outlined, the current robot control software can be improved, mainly focusing on additional checks to deliver HIFU therapy inside the ThxOF and with sufficient time between subsequent shots. 3D mouse control for initial positioning of the transducer is expected to improve HIFU workflow and identification of the target artery in all image planes. However, 3D mouse control requires training and experience and a calibration is required prior to HIFU therapy to increase intuitively. Visualizations can be improved by adding (3D) orientation markings for transducer orientation. To increase robot safety in the future, the robot control software should be able to display the force exerted by the UR3s distal end and provide active feedback if robot force or motion towards the patient is reaching a predefined threshold, as currently implemented for robot translations and rotations.

6.2 Future outline

Besides the outlined improvements of the current software, future improvements of the robotic setup should focus on the implementation of pretreatment planning and semiautomatic robot navigation during a HIFU procedure. During one animal experiment, magnetic resonance imaging of the femoral arteries was performed prior to HIFU therapy. Additionally, a Microsoft Kinect was used to capture depth images of the UR3 robot and the DMUA-transducer with respect to the porcine model. ECG markers functioned as reference positions, as they were visible on both the MRI images, as well as the depth images of the Microsoft Kinect.

Using markers placed on the pig's skin parallel to the target artery with predefined mutual distances, pretreatment planning can be performed by measuring the perpendicular distance between the markers and the target artery using the preoperational MRA. During a HIFU procedure, the robot can be moved to the reference markers, and the required robot poses between the markers can be calculated for 1 mm 3D linear spacing between subsequent treatment planes. The measured artery depth should correspond to the required axial HIFU coordinates. Using the Microsoft Kinect as optical tracker, a 3D change in relative transducer position with respect to the target area can be monitored during a procedure. If the target area moves, or the transducer position changes unintentionally, the Kinect can be used to monitor the change in relative positions. Subsequently, the calculated robot poses corresponding to each treatment plane can be recalculated.

Atherosclerotic plaque targeting can be advanced significantly in the future with an integrated HIFU and robot control system, if multiple HIFU shots at different locations can be delivered within each treatment plane at once and when pretreatment planning is combined with active positioning feedback during HIFU therapy to semi automatically navigate the transducer with respect to the desired therapy locations.

Conclusion

The feasibility of robotic transducer control to target atherosclerotic plaques was demonstrated using a six-DOF robot. Custom robot control software was designed and implementing, enabling transducer translations and orientations in three orthogonal direction (x, y and z). 2D and 3D visualizations of each HIFU ablation position improved positioning and monitoring during treatment, as well as real-time distance feedback for subsequent ablations. The robot's accuracy and repeatability were found to be within the desired range for robot translations and rotations. The exerted robot power at its distal end was quantified and will in the future be assessed to approve of the clinical implementation of the robot. *In vivo* use of the robot and custom software demonstrated its feasibility and potentially increased therapeutic success. Integration of the separate HIFU system and robot control system may further increase therapeutic efficacy by enabling direct feedback of the HIFU coordinates and distance between ablation positions to the HIFU operator.

A retrospective study on patients previously treated with PTA, stenting or surgical revascularization was performed to determine which patients and artery trajectories are most suitable for HIFU surgery. With the current HIFU system, ~30% of the dorsal arterial wall left and right can be targeted. Combined with observed variation in arterial tortuosity and lesion occurrence between patients, these results stress the need for careful patient selection and individual treatment planning in the future.

The feasibility of robotic transducer positioning and custom robot control software was demonstrated. Future developments should focus on combining the HIFU system and robot control system. Subsequently, the implementation of pretreatment planning, active positioning feedback and (semi)automatic robot navigation is expected to significantly improve therapeutic efficacy in the future. This research is a first step towards the clinical implementation of the robotic HIFU surgery approach for atherosclerosis, and we hope that it may eventually lead to a standardized noninvasive treatment option for patients suffering from PAD.

References

1. Townsend N, Wilson L, Bhatnagar P, Wickramasinghe K, Rayner M, Nichols M. Cardiovascular disease in Europe: Epidemiological update 2016. *Eur Heart J*. 2016;37(42):3232-3245. doi:10.1093/eurheartj/ehw334.

2. Munger MA, Hawkins DW. Atherothrombosis: Epidemiology, Pathophysiology, and Prevention. *J Am Pharm Assoc*. 2004;44(2):S5-S13. doi:10.1331/154434504322904569.

3. Hirsch AT, Haskal ZJ, Hertzer NR, et al. ACC / AHA PRACTICE GUIDELINES ACC / AHA 2005 Guidelines for the Management of Patients With Peripheral Arterial Disease (Lower Extremity, Renal, Mesenteric, and Abdominal Aortic): A Collaborative Report From the American Association. 2006;47(6). doi:10.1016/j.jacc.2005.10.009.

4. Newman AB, Shemanski L, Manolio TA, et al. Ankle-Arm Index as a Predictor of Cardiovascular Disease and Mortality in the Cardiovascular Health Study. 1999:538-545.

5. Lau JF, Weinberg MD, Olin JW. Peripheral artery disease. Part 1: Clinical evaluation and noninvasive diagnosis. *Nat Rev Cardiol*. 2011;8(7):405-418. doi:10.1038/nrcardio.2011.66.

6. Topol EJ. *Textbook of Interventional Cardiology, 5th*. Elsevier Health Sciences; 2008.

7. Almekkaway MK, Shehata IA, Ebbini ES. Anatomical-based model for simulation of HIFU-induced lesions in atherosclerotic plaques. *Int J Hyperth*. 2015;31(4):433-442. doi:10.3109/02656736.2015.1018966.

8. Cao P, Eckstein HH, De Rango P, et al. Chapter II: Diagnostic methods. *Eur J Vasc Endovasc Surg*. 2011;42(SUPPL. 2). doi:10.1016/S1078-5884(11)60010-5.

9. Jackson SP. Arterial thrombosis-insidious, unpredictable and deadly. *Nat Med*. 2011;17(11):1423-1436. doi:10.1038/nm.2515.

10. Ederle J, Brown MM. The evidence for medicine versus surgery for carotid stenosis. *Eur J Radiol*. 2006;60(1):3-7.

11. Joosten MM, Pai JK, Bertoia ML, et al. Cardiovascular Risk Factors and Risk of Peripheral Artery Disease in Men. *Am Med Assoc*. 2012;308(308):1660-1667.

12. Spronk S, Bosch L, Veen F, den Pieter T, Hunink Myriam MG. Intermittent claudication: functional capacity and quality of life after exercise training or percutaneous transluminal angioplasty - systematic review. *Radiology*. 2005;235(3):833. doi:10.1148/radiol.2353040457.

13. Miloro P, Sinibaldi E, Menciassi A, Dario P. Removing vascular obstructions: a challenge, yet an opportunity for interventional microdevices. *Biomed Microdevices*. 2012;14(3):511-532. doi:10.1007/s10544-011-9627-2.

14. Mahmud E, Cavendish JJ, Salami A. Current Treatment of Peripheral Arterial Disease. Role of Percutaneous Interventional Therapies. *J Am Coll Cardiol*. 2007;50(6):473-490. doi:10.1016/j.jacc.2007.03.056.

15. Shehata IA. Treatment with high intensity focused ultrasound: secrets revealed. *Eur J Radiol*. 2012;81(3):534-541.

16. Jenne JW, Preusser T, Günther M. High-intensity focused ultrasound: Principles, therapy guidance, simulations and applications. *Z Med Phys*. 2012;22(4):311-322. doi:10.1016/j.zemedi.2012.07.001.

17. Poissonnier L, Gelet A, Chapelon J-Y, et al. Results of transrectal focused ultrasound for the treatment of localized prostate cancer (120 patients with PSA< or+ 10ng/ml. *Prog en Urol J l'Association Fr d'urologie la Soc Fr d'urologie*. 2003;13(1):60-72.

18. Sanghvi NT, Foster RS, Bihrle R, et al. Noninvasive surgery of prostate tissue by high intensity focused ultrasound: an updated report. *Eur J Ultrasound*. 1999;9(1):19-29.

19. Gardner TA, Koch MO, Shalhav A, et al. Minimally invasive treatment of Benign Prostatic Hyperplasia with High Intensity Focused Ultrasound using the Sonablate System: an updated report of Phase III clinical studies conducted in the USA. In: *Lasers in Surgery: Advanced Characterization, Therapeutics, and Systems XII*. ; 2002.

20. Dewhirst MW, Viglianti BL, Lora-Michiels M, Hanson M, Hoopes PJ. Basic principles of thermal dosimetry and thermal thresholds for tissue damage from hyperthermia. *Int J Hyperthermia*. 2009;19(3):267-294. doi:10.1080/0265673031000119006.

21. Sapareto SA, Dewey WC. Thermal dose determination in cancer therapy. *Int J Radiat Oncol Biol Phys*. 1984;10(6):787-800. doi:10.1016/0360-3016(84)90379-1.

22. Dubinsky TJ, Cuevas C, Dighe MK, Kolokythas O, Hwang JH. High-intensity focused ultrasound: current potential and oncologic applications. *AJR Am J Roentgenol*. 2008;190(1):191-199. doi:10.2214/AJR.07.2671.

23. ter Haar G, Coussios C. High intensity focused ultrasound: Physical principles and devices. *Int J Hyperth*. 2007;23(2):89-104. doi:10.1080/02656730601186138.

24. Siegel RJ, Fishbein MC, Forrester J, et al. Ultrasonic Plaque Ablation. *Circulation*. 1988;78:1-6.

25. Fischell TA, Abbas MA, Grant GW, Siegel RJ. Ultrasonic energy. Effects on vascular function and integrity. *Circulation*. 1991;84(4):1783-1795. doi:10.1161/01.CIR.84.4.1783.

26. Rosenschein U, Bernstein JJ, DiSegni E, Kaplinsky E, Bernheim J, Rozenzsajn LA. Experimental ultrasonic angioplasty: Disruption of atherosclerotic plaques and thrombi in vitro and arterial recanalization in vivo. *J Am Coll Cardiol*. 1990;15(3):711-717. doi:10.1016/0735-1097(90)90651-5.

27. Xianhong S. Ultrasound Disruption of Atherosclerotic Plaques in Vitro Study. *CHINESE J ULTRASOUND Med*. 1996:1.

28. Goertz DE. An overview of the influence of therapeutic ultrasound exposures on the vasculature: High intensity ultrasound and microbubble-mediated bioeffects. *Int J Hyperth*. 2015;31(2):134-144. doi:10.3109/02656736.2015.1009179.

29. Munger MA, Hawkins DW. Atherothrombosis: epidemiology, pathophysiology, and prevention. *J Am Pharm Assoc*. 2004;44(2):S5--S13.

30. ter Haar G. Therapeutic applications of ultrasound. *Prog Biophys Mol Biol*. 2007;93(1-3):111-129. doi:10.1016/j.pbiomolbio.2006.07.005.

31. ter Haar GR. High intensity focused ultrasound for the treatment of tumors. *Echocardiography*. 2001;18(4):317-322. doi:10.1046/j.1540-8175.2001.00317.x.

32. Kim H-J, Kim HG, Zheng Z, et al. Coagulation and ablation patterns of high-intensity focused ultrasound on a tissue-mimicking phantom and cadaveric skin. *Lasers Med Sci*. 2015;30(9):2251-2258. doi:10.1007/s10103-015-1804-8.

33. ter Haar GR, Robertson D. Tissue Destruction with Focused Ultrasound in vivo. *Eur Urol*. 1993;23(suppl 1:8-11. https://www.karger.com/DOI/10.1159/000474672.

34. Dogra VS, Zhang M, Bhatt S. High-Intensity Focused Ultrasound (HIFU) Therapy Applications. *Ultrasound Clin*. 2009;4(3):307-321. doi:10.1016/j.cult.2009.10.005.

35. Kim Y, Rhim H, Choi MJ, Lim HK, Choi D. High-Intensity Focused Ultrasound Therapy: an Overview for Radiologists. *Korean J Radiol*. 2008;9(4):291. doi:10.3348/kjr.2008.9.4.291.

36. Tashtoush A. High intensity focused ultrasound (HIFU) technique for ablation of various disease treatments guided by ultrasound. *Int J Simul Syst Sci Technol*. 2016;17(33):1.1-1.7. doi:10.5013/IJSSST.a.17.33.01.

37. Maleke C, Konofagou EE. Harmonic motion imaging for focused ultrasound (HMIFU): a fully integrated technique for sonication and monitoring of thermal ablation in tissues. *Phys Med Biol*. 2008;53(6):1773-1793. doi:10.1088/0031-9155/53/6/018.

38. Ballard JR, Casper AJ, Liu D, et al. Dual-mode ultrasound arrays for image-guided targeting of atheromatous plaques. In: *AIP Conference Proceedings*. Vol 1503. 2012:124-128. doi:10.1063/1.4769929.

39. Ballard JR, Casper AJ, Ebbini ES. Monitoring and guidance of HIFU beams with dual-mode ultrasound arrays. *Proc 31st Annu Int Conf IEEE Eng Med Biol Soc Eng Futur Biomed EMBC 2009*. 2009:137-140. doi:10.1109/IEMBS.2009.5334677.

40. Shehata IA, Ballard JR, Casper AJ, Liu D, Mitchell T, Ebbini ES. Feasibility of targeting atherosclerotic plaques by high-intensity-focused ultrasound: An in vivo study. *J Vasc Interv Radiol*. 2013;24(12):1880-1887.

41. Liu D, Casper A, Haritonova A, Ebbini ES. Adaptive lesion formation using dual mode ultrasound array system. *AIP Conf Proc*. 2017;1821:1-6. doi:10.1063/1.4977627.

42. Davies BL, Chauhan S, Lowe MJS. A robotic approach to HIFU based neurosurgery. *Med Image Comput Comput Interv - MICCAI'98*. 1998;1496:386-396. doi:10.1007/BFb0056181.

43. Chauhan S, Ter Haar G. FUSBOTUS: Empirical studies using a surgical robotic system for urological applications. *AIP Conf Proc*. 2007;911:117-121. doi:10.1063/1.2744261.

44. Susanto S, Chauhan S. A hybrid control approach for non-invasive medical robotic systems. *J Intell Robot Syst Theory Appl*. 2010;60(1):83-110. doi:10.1007/s10846-010-9407-x.

45. An CY, Syu JH, Tseng CS, Chang CJ. An ultrasound imaging-guided robotic HIFU ablation experimental system and accuracy evaluations. *Appl Bionics Biomech*. 2017;2017. doi:10.1155/2017/5868695.

46. Hynynen K. MRIgHIFU: A tool for image-guided therapeutics. *J Magn Reson Imaging*. 2011;34(3):482-493. doi:10.1002/jmri.22649.

47. Sherwood V, Civale J, Rivens I, Collins DJ, Leach MO, Ter Haar GR. Development of a Hybrid Magnetic Resonance and Ultrasound Imaging System. *Biomed Res Int*. 2014;2014. doi:10.1155/2014/914347.

48. Napoli A, Anzidei M, Ciolina F, et al. MR-Guided High-Intensity Focused Ultrasound: Current Status of an Emerging Technology. *Cardiovasc Intervent Radiol*. 2013;36(5):1190-1203. doi:10.1007/s00270-013-0592-4.

49. Mauri G, Cova L, De Beni S, et al. Real-Time US-CT/MRI Image Fusion for Guidance of Thermal Ablation of Liver Tumors Undetectable with US: Results in 295 Cases. *Cardiovasc Intervent Radiol*. 2015;38(1):143-151. doi:10.1007/s00270-014-0897-y.

50. Ebbini ES, Ter Haar G. Ultrasound-guided therapeutic focused ultrasound: Current status and future directions. *Int J Hyperth*. 2015;31(2):77-89. doi:10.3109/02656736.2014.995238.

51. Chauhan S, Tan MT, Seet G, Ng I. Minimally invasive robotic HIFU neurosurgical applications. *Proc 38th Annu Symp Ultrason Ind Assoc UIA 2009*. 2009:1-5. doi:10.1109/UIA.2009.5404033.

52. Price KD, Sin VW, Mougenot C, et al. Design and validation of an MR-conditional robot for transcranial focused ultrasound surgery in infants. *Med Phys*. 2016;43(9):4983-4995. doi:10.1118/1.4955174.

53. Masamune K, Kurima I, Kuwana K, Yamashita H, Chiba T, Dohi T. HIFU positioning robot for less-invasive fetal treatment. *Procedia CIRP*. 2013;5:286-289. doi:10.1016/j.procir.2013.01.056.

54. Casper AJ, Dalong Liu, Ballard JR, Ebbini ES. Real-Time Implementation of a Dual-Mode Ultrasound Array System: In Vivo Results. *IEEE Trans Biomed Eng*. 2013;60(10):2751-2759. doi:10.1109/TBME.2013.2264484.

55. Universal Robots. (2018). *User Manual UR3/CB3 Version 3.1 (rev. 17782)*. Retrieved from https://www.universal-robots.com/media/207442/ur3_user_manual_en_global.pdf.